REVIEW

Check for updates

Nanoscale designing of metal organic framework moieties as efficient tools for environmental decontamination

Indu Sharma,†[a] Jaspreet Kaur,†[b] Gargi Poonia,[a] Surinder Kumar Mehta [ID] *[a] and Ramesh Kataria [ID] *[a]

Environmental pollutants, being a major and detrimental component of the ecological imbalance, need to be controlled. Serious health issues can get intensified due to contaminants present in the air, water, and soil. Accurate and rapid monitoring of environmental pollutants is imperative for the detoxification of the environment and hence living beings. Metal–organic frameworks (MOFs) are a class of porous and highly diverse adsorbent materials with tunable surface area and diverse functionality. Similarly, the conversion of MOFs into nanoscale regime leads to the formation of nanometal–organic frameworks (NMOFs) with increased selectivity, sensitivity, detection ability, and portability. The present review majorly focuses on a variety of synthetic methods including the *ex situ* and *in situ* synthesis of MOF nanocomposites and direct synthesis of NMOFs. Furthermore, a variety of applications such as nanoabsorbent, nanocatalysts, and nanosensors for different dyes, antibiotics, toxic ions, gases, pesticides, *etc.*, are described along with illustrations. An initiative is depicted hereby using nanostructures of MOFs to decontaminate hazardous environmental toxicants.

1. Introduction

The rapid upsurge of pollutants is raising a red alert for the healthy living of the species present worldwide. The presence of organic waste, various toxic gases from industries (CO_2, SO_2, NO_2, H_2S, *etc.*), dyes from textile industries, oils, and detergents in the environment are endangering flora and fauna.[1] About 80% of 1.3×10^5 tons of active dyestuff produced is used in the textile industries of India, which is a matter of great concern.[2] Moreover, heavy metals, having a high atomic weight and 5 times higher density than water, contain a high degree of toxicity. These heavy metal ions including Hg, Pb, Cr, and Cd above their safe threshold may cause serious diseases including acute or chronic poisoning by their exposure to food, air, and water.

Along with heavy metal ions, certain pharmaceuticals, pesticides, antibiotics, herbicides, and insecticides are captivating the research interest due to their adverse impact on the ecosystem. These contaminants degrade soil and water quality by mixing into them. Various personal care products (PCPs), such as diclofenac, musks, carbamazepine, ibuprofen, and bisphenol A, were listed as emerging components according to

the priority pollution list by EU (European Union) and USEPA (United States Environmental Protection Agency) in 2007.[3] Several gases released from domestic, agricultural, and industrial fields are responsible for climate change by increasing the ocean and earth's temperature.[4] Emerging contaminants (ECs), also known as micropollutants, are a diverse group of anthropogenic substances that are frequently found in water but have only recently been recognized as significant contaminants in water.[5] The generation of these pollutants has increased from one million to 500 million tonnes annually throughout the world.[6] Nevertheless, many ECs have been linked to known or suspected negative effects on human health and the environment, as shown in Fig. 1(a).[7,8] Fig. 1(b) outlines the various ECs posing threats to the human environment. These pollutants primarily come from industrial, agricultural, and municipal wastewater as well as industrial smoke because water and air may easily migrate from one site to another. Fig. 1(c) depicts the life-cycle distribution of emerging micropollutants from the perspective of sources to receptors.

The ecological balance is based upon the interaction of society with the environment. The behavior of society with the environment majorly influences the health of the ecosystem. Several responses given by our society to the environment using the above-described contaminants are accompanied by climate change, toxicity in air, soil infertility, adverse aquatic environment, and so on. There is a crucial need to overcome these challenges as there is no question of our existence if we are

[a]*Department of ChemistryCentre of Advanced Studies in Chemistry, Panjab University, Chandigarh-160 014, India. E-mail: skmehta@pu.ac.in; rkataria@pu.ac.in*

[b]*School of Basic Sciences, Indian Institute of Information Technology (IIIT), Una-177 209, India*

† Equal contribution of authors.
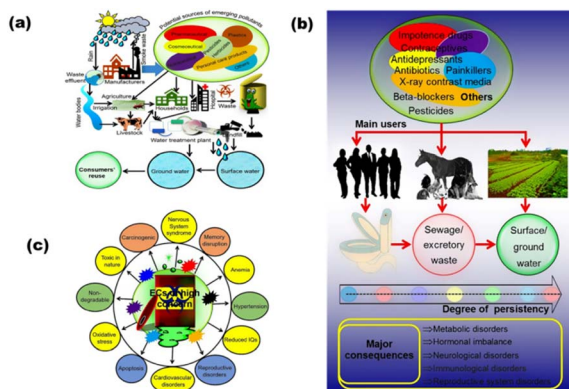
Fig. 1 (a) Subsequent distribution of arising pollutants from sources to the receptors, (b) schematic representation of the sources of various pharmaceutical drugs, their prime consumers, persistency and their major outcomes, and (c) adversity of various ECs for human beings and environment (reproduced with permission from ref. 7. Copyright 2019 Elsevier).

prone to an endangered life full of such environmental threats. To date, there are numerous researches done in the same field.

MOFs, metal centers linked with various multitopic organic linkers have currently been classified as an important group consisting of porous compounds. MOFs can possess various features, *e.g.*, large surface area, enhanced pore volume, linking abilities, and tunable structure architecture. A zeolite-imidazole-based family of MOFs termed ZIF (Zeolite Imidazole Framework) family consist of metal centers Fe, Cu, Co, *etc.*, surrounded by imidazole connectivity. Moreover, UIL, HKUST, MIL, *etc.*, are also some of the families of MOFs accompanying a large number of MOFs with them.[9] To restrict various metal ions in the ZIF9 framework, a novel space-confined synthesis technique is provided.[10] By performing high-temperature pyrolysis, a variety of carbon compounds generated from ZIF9 that exhibit high capacitance and high rates of charge transfer were produced. Capacitive deionization (CDI) encourages the creation of carbon materials produced by MOF for use in the domains of water and energy treatment, which have a wide range of potential applications. MOFs are in demand nowadays for their extended applicability in the field of environmental decontamination through the use of their gas sensing, catalytic, and adsorptive properties along with luminescent sensing properties.[11] In addition, MOF-based biosensors and fluorescent sensors have been developed nowadays due to various naturally-occurring transitions in between them.[12]

Despite having many advantageous features, there occur some substantial drawbacks, *e.g.*, poor mechanical strength and electrical conductivity, slow degradation, and less resistance toward water and light.[9] Hence, to improve the abovementioned properties, it is necessary to convert MOFs to their corresponding nanostructures (nanoparticles/nanocomposites). Various carbon-based hybrid nanocomposites have drawn the attention of researchers for environmental decontamination. CNT (carbon nanotubes) have evolved as an effective adsorbent over activated carbon, fly ash, and zeolite due to their tunable adsorption capacity and surface chemistry. Their usage is limited due to

their cost; hence, nanocomposites are made using MOFs with carbon-based materials such as CNTs, graphene, and rGO. Carbon nanocomposites can improve the mechanical strength and chemical stability of MOFs. The surface area reported from BET analysis was 7000 m^2 g^{-1}, which was much more than that of bare MOFs.[13] Similarly, the encapsulation of metal NPs (Ag, Pt, Pd, Fe, *etc.*) and metal oxide NPs have also been done by researchers, *e.g.*, Bi$_2$O$_3$@HKUST-1, ZnO@ZIF-8, UiO-66@WO$_3$, and Fe$_3$O$_4$@MIL(100) as photocatalysts.[14] Semiconductors such as TiO$_2$, g-C$_3$N$_4$, CdSe, GaP, ZnS, and CdS also evolved in this field to combine the properties of MOFs and semiconductors for their better photocatalytic abilities. This is due to the facile transfer of charges, water, and light through these nanocomposites as compared to their bare constituents.[15]

Herein, various MOF nanostructures including nanoparticles and nanocomposites have been reviewed as environmental decontaminants. This present review emphasizes various *ex situ* and *in situ* methods of synthesis of MOF nanocomposites with carbon materials, metal nanoparticles (MNPs), metal oxides, and semiconductors. The direct synthesis of MOF nanoparticles using various methods including solvothermal, ultrasonic, electrochemical, and microwave-assisted has also been illustrated here. MOF nanostructures were employed as nanocatalysts, nanosensors and nanoadsorbents for different toxic ions, gases, dyes, antibiotics, and pesticides. Relevant classification, explanation, and suitable illustrations for each synthetic strategy and applicability of NMOFs are described in this paper. The outline of the recount has been depicted in Scheme 1.

2. Synthesis

2.1. Direct synthesis of MOF nanoparticles (MOF NPs)

The assembly of metal ions and ligands to form MOFs depends upon the solvents, reaction time, and temperature. Catalytic site
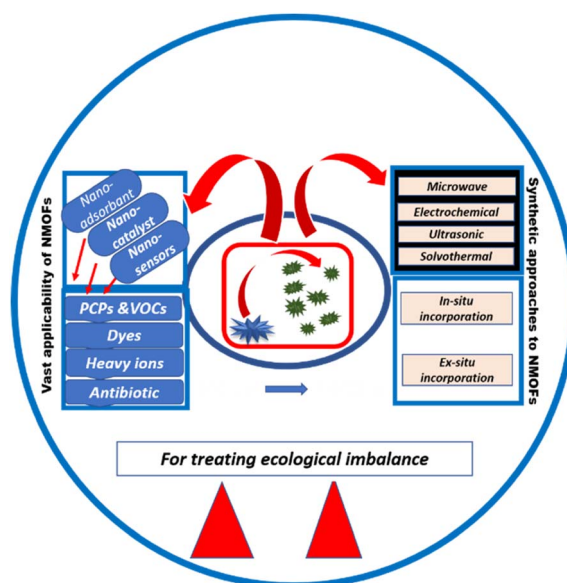
Scheme 1 Schematic representation for the layout of the description given in the paper.

production for the reaction is influenced by the solubility of reactants and temperature while the final morphology of the NMOFs is decided by the affinity between the ligands and metal centers. The better the solubility of the reacting species, the more will be the emergence of nanoscale units. Template method or using emulsions can also promote the formation of nanoscale MOFs by limiting the size of self-assembling species. Herein, some methods are described to directly synthesize nanoscale MOFs, namely, microwave assistance, solvothermal process, electrochemical synthesis, and ultrasonic synthesis.

2.1.1 Microwave-assisted approach. The microwave-assisted method is environment-friendly and a large-scale production method having lesser reaction time. Electromagnetic waves interact directly with the moving charges in reactants to impart energy. The mobile charges come from polar molecules, electrons, or ions from solvent. There occurs an increase in kinetic energy due to some collisions among the molecules that are in resonance with microwave frequency. There are two types of acoustic cavitation—transient and stable cavitation. The microstreaming phenomenon that results from stable cavitation causes bubbles to oscillate regularly for several acoustic cycles, stressing the microorganisms shown in Fig. 2(a). Transient cavitation occurs when bubbles are generated and go through irregular oscillations that result in the regions of temperature and pressure change shown in Fig. 2(b), which kills cells and renders enzymes inactive.[16] The increased kinetic energy is transformed into the form of heat energy. Microwave power, reaction time, and concentration of reactants determine the dimensions and size range of NMOFs.[17,18] The major advantages of this method are excellent sample crystallinity and purity, increased reaction time, *i.e.*, less than an hour and low reaction system temperature.[19]

Chalati *et al.* synthesized nanoparticles of a porous and flexible iron-based MOF, *i.e.*, MIL-88A using various synthesis schemes. The yield and particle size of the MOF were analyzed using static hydrothermal/solvothermal synthesis, ultrasonic synthesis, dynamic ambient pressure synthesis, and microwave-assisted synthesis conditions. Only microwave-assisted hydrothermal synthesis proved to be the most rapid and convenient

method to control the size along with larger yields of mono-dispersed nanoparticles, *i.e.*, size less than 100 nm and poly-dispersity index [PDI] less than 0.20. While using ultrasonic synthesis, a mediocre yield of monodispersed MOF nano-particles was obtained with a size of 100 nm and PDI of 0.24.[20] Further, flower-like nanostructures of Ta-MOF have also been successfully achieved using ultrasound-assisted microwave irradiation.[21] There is no evidence of particle agglomeration or aggregation when employing the ultrasound-assisted method since the sample produced by this approach has a more consistent morphology than the sample produced by the microwave method. However, the microwave technique results in some particle aggregation, which can increase the Ta-MOF sample's diameter.

2.1.2 Electrochemical synthesis. Electrochemistry has been emerging as an efficacious technique for the production of MOFs.[22] The metal source for the electrochemical synthesis of MOFs is produced from a sacrificial metal anode by an electric field.[23] As a result, the metal serves as the reaction system's anode, while the cathode might utilize different inert electrodes or the same material as the anode.[24,25] Metal ion deposition from the anode onto the cathode gets suppressed on using protic solvents in the reaction mixture.[26] The composition of the solvent, voltage, and reaction time are the key influencing elements for the electrochemical synthesis of MOFs in the available literature (Fig. 3).[27] NMOFs synthesis by electrochemical synthesis needs no addition of external metal salt/solutions but anode dissolution for the metal source. The reaction yields high solid produce after some hours at room temperature, keeping some parameters under control. The controlling parameters include the nature of the solvent and electrolyte, the temperature of the producer, and voltage–current density.

Zhang *et al.* synthesized nanoparticles of a Zn-based Iso-Reticular MOF (IRMOF-3) having Zn_4O as a secondary building unit and NH_2–H_2 BDC (2-aminoterephthalic acid) as linkers. The synthesis was completed within 3 h using the electrochemical method. After the passage of 3 h and at 6 V voltage, the synthesized NMOFs were found to have a size less than 200 nm. The products were amorphous when pure DMF was taken as the solvent.
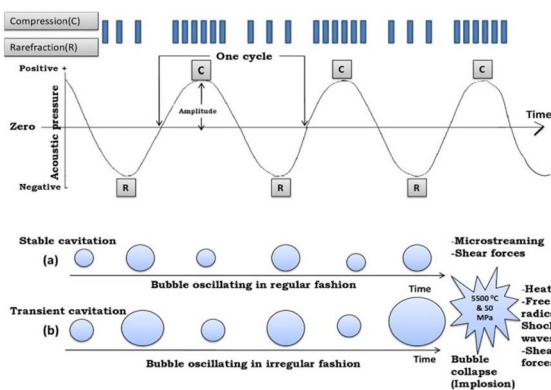

Fig. 2 Mechanism showing cavitation phenomenon: (a) stable cavitation and (b) transient cavitation (reproduced with permission from ref. 16. Copyright 2019 Elsevier).
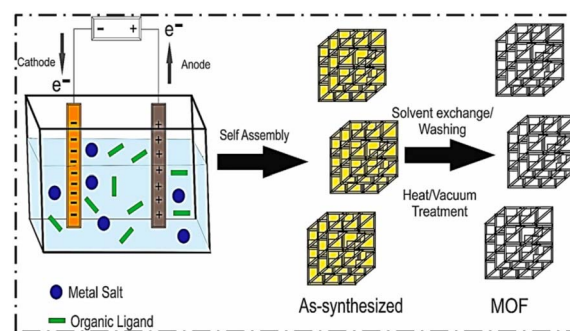

Fig. 3 Schematic diagram of the electrochemical synthetic procedure of MOFs (reproduced with permission from ref. 27. Copyright 2020 Elsevier).

After adding ethanol with DMF slowly, the XRD pattern of NMOFs was found to match the simulated pattern. The reason behind this was that the nucleation rate was affected by ethanol. The concentration of ethanol should be kept low, keeping in view that the concentration of reactants should be comparable. Moreover, they also synthesized polyhedral NMOF (UiO-66-NH$_2$) of size 65 nm with a reaction time of 1 h and at 4 V voltage. The solvent used was DMF and acetic acid in a ratio of 52 : 8. Although this strategy takes a few hours for the reaction to complete but it proves to be cost-effective and occurs at normal pressure and temperature for the direct synthesis of NMOFs.[19–28]

2.1.3 Solvothermal process. This method includes the reaction in a closed autoclave at high pressure and temperature greater than the boiling point of the used organic solvent. The process of crystallization and growth of nanoparticles is governed by a CNT-based homogeneous nucleation model named LaMer. The process is comprised of four basic steps: first, enhancement in the concentration of the reacting species in the solution; second, after exceeding the critical nucleation concentration, there is an emergence of homogeneous nucleation; third is the rapid decline in monomer concentration; and finally, the synthesized crystal initiates the extended growth after attaining saturated concentration for getting highly crystalline and pure NMOFs. The morphologies and particle size of the NMOFs can be modulated by regulating certain criteria such as time of reaction, concentration of reacting species, and temperature.[19] Using the solvothermal method, the quickest recorded time for the synthesis of HKUST-1 MOF using a conductively heated reactor was achieved.[29] The reaction yields were about 84% and 100%. Since the particle size was discovered to be in the nanometric range in this work and monocrystalline nanoparticles may have been present, a synthesis period of 10 min showed the most intriguing characteristics. An improvement in its existing uses, such as photocatalysis, storage, pollutants removal, or drug delivery, may be anticipated due to the substantial degree of crystallization, acquired particle size, and optoelectronic properties.

Behrens et al. used the solvothermal method that studied the size regulation of Zr-MOF NPs by regulating the reagent concentration. After adding different ratios of benzoic acid, the size of Zr-MOFs could be regulated. With the enhancement in benzoic acid concentration, the aggregation of smaller particles to single nanocrystals takes place gradually, as revealed by scanning electron microscopy (SEM) analysis. In the end, good crystal shapes with 200 nm size were obtained after using 30 times the equivalent of benzoic acid to ZrCl$_4$.[30]

2.1.4 Ultrasonic synthesis. The use of ultrasonic waves provides NMOFs without the involvement of surface residue washing and fabricates a comparatively smoother surface. It is a rapid and quite simple process that depends upon the interaction between the reacting liquids and ultrasonic waves. Here, liquids are used as reactants rather than molecules because there is a lack of proper resonance between ultrasonic waves and molecules as the wavelength of ultrasonic waves is much higher than that of the molecules. The acoustic cavitation and crumbling bubbles are the main reason behind the emergence
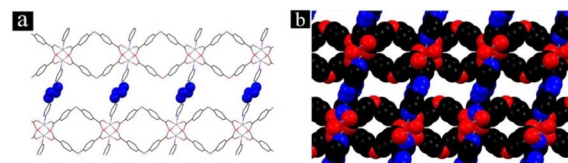

Fig. 4 (a) Stick cap model and (b) space-filled model showing the interconnected pores for the representation of TMU-34(-2H) (reproduced with permission from ref. 31. Copyright 2017 Elsevier).

of chemical reactions by the use of ultrasound waves. This acoustic cavitation improves the activity of the reactants by inducing tremendously high temperature, i.e., 5000 K, cooling rate, i.e., 1010 K s^{-1} and pressure at 1800 atm.[19]

TMU-34(-2H) MOF powder was synthesized by the sonochemical method shown in Fig. 4.[31] The pink powder was characterized using IR spectroscopy, X-ray powder diffraction, scanning electron microscopy, and N$_2$ adsorption.

For the morphological modification, the initial concentration of reagents, molar ratio of pyridine, sonication time, and power were optimized. The SEM images of the synthesized compound after 60, 80, and 100 min were recorded, as shown in Fig. 5. The outcomes indicated that TMU-34(-2H) exhibits a uniform plate-like morphology at 360 W power and 60 min sonication time with pyridine as the modulator.

Qiu et al. used an ultrasonic technique to synthesize nanoparticles of Cu-BTC [Cu(II)-benzene-1,3,5-tricarboxylate] MOF within the size range from 50 to 100 nm. Within 10 min, the yield of MOF NPs was found to be 78.2% while reaching 85.3% with the increase in reaction time. The size-controlling parameters were the addition of inhibitors, dilution, and a decrease in temperature.[32] Using the ultrasonic method, Zn(II)-based nanoparticles of MOF (TMU-4) with a reaction time of 5 to 10 min and a size range of 50 to 100 nm were fabricated by Morsali et al. Most optimized and uniform nanostructures were obtained after 90 min with a pH regulator concentration of 0.02 mol L^{-1}. The Zn-MOF NPs were facile to synthesize at room temperature. They include some features including photodegradability and high uniformity.[33]

2.2. In situ incorporation of NPs in MOFs

MOFs have a vast variety of applications including adsorption, catalysis, sensing, gas storage, gas–vapor separation, and biomedical imaging. The conversion of MOFs to their nanostructures can be an efficient tool to improve their morphology,
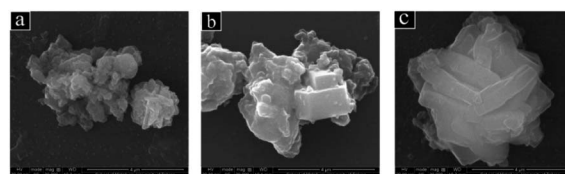

Fig. 5 SEM images of sonochemically synthesized TMU-34(-2H) after (a) 60 min, (b) 80 min, and (c) 100 min (reproduced with permission from ref. 31. Copyright 2017 Elsevier).

surface area, porosity, and uniformity, and hence enhances their applicability. MOF nanoparticles can be synthesized by various methods. Among them, *in situ* encapsulation is one of the efficient methods that can be adopted due to its low complexity and lesser reaction time. This process provides us with more thermostability, particularly MOFs. In comparison to other synthetic strategies, this method provides effective and more guest component-loading over the host MOF. The guest components may include metal oxide and metal nanoparticles (MNPs). There are various *in situ* methods for the synthesis of MOF nanoparticles. Some of them are solvothermal, hydrothermal, electrospun, microwave synthesis, the deligandation process, polymerization, spin coating, and thermal crosslinking.

Herein, we have discussed some of the methods for the *in situ* synthesis of MOF nanostructures, *e.g.*, solvothermal method, hydrothermal method, and electrospun method.[34]

2.2.1 Solvothermal method. The temperature of the reaction is a crucial factor in the production of MOFs.[35] The solvothermal method encourages the reaction and operates the process of crystallization, and the acquired MOF materials typically have high heat stability. Solvothermal reactions are carried out in confined vessels at medium pressure and temperatures above the boiling point of the solvent. Crystalline materials are produced through solvothermal synthesis by creating a high-pressure surrounding by raising the temperature above the reactants' boiling point in a closed reaction system.[36] Using standard electric heating, the reactions of synthesis are usually carried out without any correlation with standard synthesis techniques. In addition, its principle is primarily manifested as the chemical substances react from the predecessor to the crystal due to the change in the solubility of the pressure vessels. The gradient of temperature that is created between the crystallization zones and dissolution is responsible for the change in solubility.[37]

However, during the growth of the crystals, chemical and structural defects are frequently observed, which can be tuned by altering the crystal growth rate of the solvothermal process. In addition, the crystal growth rate can be enhanced by adjusting the pressure, reaction temperature, growth temperature, crystal orientation, solvent concentration, and hydrodynamics.[38] As a result, optimizing the parameters of growth rate allows solvothermal synthesis to control the morphology of the crystals derived. Miyamoto *et al.* used a solvothermal method for the growth of UiO-66 films using monocrystalline growth of UiO-66 nanocrystals. Adding acetic acid and water influenced the synthesis of a highly oriented film of UiO-66. Acetic acid controlled the crystal growth by acting as a modulator while water accelerated Zr precursor hydrolysis and thereby enhanced UiO-66 intergrowth without influencing their orientation. The reported UiO-66 film containing excellent orientation of crystals displayed higher chemical stability than that of MOF(UiO-66) powder. Further, SEM images revealed the highly-oriented monocrystalline growth of the film. Based on chemical stability and high orientation, these films were expected to show excellent applicability compared to bare MOF UiO-66.[39]

2.2.2 Hydrothermal method. A technique that makes use of water (solvent) is referred to as the hydrothermal method. For a particular structure, various synthesis factors, including temperature, pressure, reagent concentration, and solvent composition, are adjusted.[40] The autoclave is a specialized equipment used for hydrothermal synthesis. In it, a temperature gradient is nurtured between growth chambers at opposite ends, and the precursor and water as solvent are supplied. Hydrothermal synthesis is the method by which the synthetic process is carried out in a solvent other than water. The size, shape, and crystallinity of the nanostructures are significantly influenced by the reaction conditions.[41] This simplicity of the present method, high product crystallinity, and high yield are its primary advantages. Metal oxides such as the Cu_2O/CuO composite, zirconium oxide (nanoparticles), gamma aluminium oxide, titanium oxide (nanoparticles), and a hollow sphere of Co_3O_4 were made by hydrothermal synthesis using a template to precisely control the crystallinity, shape distribution, and size.[42,43]

The hydrothermal method is now a widely used process in the fabrication of a broad range of materials, including bulk crystals and size-controlled and morphological nano and fine particles. When compared to more conventional methods of processing materials, the hydrothermal method offers numerous advantages.

Xu *et al.* reported the successful fabrication of Fe-MOF/Au-8/FF nanorods using the hydrothermal strategy shown in Fig. 6. This method involves the combination of an Fe foam template with electrodeposition. The nanorods were accompanied by well-resolved lattice fringes after the electrodeposition of Au. Fe-MOF, after *in situ* growth on the FF surface, undergoes electrodeposition of Au on the Fe-MOF/FF surface. This nanocomposite possesses enhanced activity due to increased conductivity, increased electrochemical activity for specific areas, and oxygen evolution (OER) and hydrogen evolution (HER).[44]
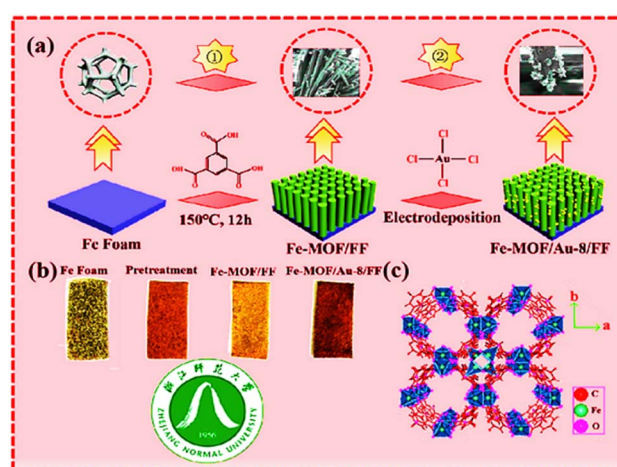

Fig. 6 (a) Schematic illustration of Fe-MOF/Au-8/FF; (b) process chart of the color change of the synthesized sample; (c) crystal structure of Fe-MOF (along *c*-axis) (reproduced with permission from ref. 44. Copyright 2022 Elsevier).

© 2023 The Author(s). Published by the Royal Society of Chemistry

Aslam et al. devised the utilization of a step-in situ hydro-thermal strategy for the efficient synthesis of Fe$_3$O$_4$@MIL-100(Fe) nanoparticles. Fe$_3$O$_4$ not only provides a magnetic core for nanocomposite growth but also provides Fe^{3+} for the heterogeneous growth of MOF MIL-100(Fe). The prepared nanocomposites showed enhancement in pore volume and surface area with the special addition of a superparamagnetic feature. These features make this nanocomposite possess a wide application field rather than its bare components, i.e., Fe$_3$O$_4$ and MIL-100(Fe). In this work, methylene blue (MB) adsorption was shown by this nanocomposite for depolluting water. The schematic representation of the work has been shown in Fig. 7.[45]

Further, in the same field, a one-pot hydrothermal method-ology was adopted to synthesize a composite consisting of cobalt oxide nanocubes dispersed over the sheet of Co-MOF (Co$_3$O$_4$@Co-MOF).[46] The composite was found to show enhancement in alkaline stability, increment in redox ability, and an expeditious increase in the capacitance value. Moreover, the integration of metal oxide with the MOF did not alter the original identity of the MOF but enhanced its applicability.

2.2.3 Electrospun method. MOFs are crystalline materials having pores and can be used as a storehouse of energy and for its conversion; however, due to a lack of interconnectivity between their porous form and easy accumulation, electron transmission can be inhibited. Thus, the electrospinning method needs to be introduced. In this technique, nanofibers at high voltage are drawn through a viscoelastic fluid, which can be accommodated to overcome the incompatibility factor between them. However, MOF nanofibers for the storage of energy and its conversion are not well recognized. The electro-spinning method used to accomplish MOFs-based nanofibers for their essential storage of energy and its conversion is of great use. Herein, we have discussed the synthesis of MOF-based nanoparticles through the electrospinning technique.[47]

Al-Baadani et al. demonstrated the use of the in situ elec-trospun method for the fabrication of Zr-based MOF (ZIF-8) nanofibers. Herein, the embedment of the polycaprolactone/gelatin (PG)-blended membrane was done with alendronate-loaded ZIF-8 (Aln/ZIF-8). Various compositions of ZIF-8 were taken, i.e., 0.25%, 0.5%, and 1%. SEM analysis revealed that the nanofibers are uniform in size and are randomly distributed without the bead defect. It further suggested the successful synthesis of nanofibers (PG/Aln-ZIF-8) with good mechanical strength.[48]

2.3. Ex situ incorporation/composites of NPs in the MOFs

It is necessary to refine the properties of MOFs for enhancing the quality of application. Eventually, various strategies to form MOF nanocomposites have been proposed, where some external entities in addition to MOF proceed toward the formation of nanocomposites of MOF. Herein, ex situ methods to form MOF nanocomposites have been detailed, including MOF loading by metal nanoparticles (MNPs), incorporation of semiconductor nanosheets into MOF, and decoration of MOFs by r-GO.

There are many methods of ex situ formation of MOF nanocomposites which can be broadly divided into three parts: (1) metal nanoparticle [MNP] loading on MOF, (2) embedding semiconductors into MOF, and (3) adorning of MOF by carbon materials.

2.3.1 Metal nanoparticle (MNP) loading. Metal nano-particle loading on MOFs can provide efficient nanocomposites with improved application, especially in photocatalysis. This strategy includes several methods such as (a) immersing MOFs in metal salt solutions following UV irradiation or reduction; (b) irradiating microwaves on a mixture containing MOF and metal precursors; (c) solid grinding process using MOFs and metal precursors.[49]

After the synthesis of various nanocomposites, certain investigations become important to ensure the proper embed-ment of MNPs within the MOFs. These include some charac-terization method listed below to reveal the actual relationship between metal-loaded MOF, i.e., nanocomposites, and unloa-ded MOF. The characterizations include – (a) TEM/SEM/PXRD to ensure the maintenance of the actual shape and crystal-linity of MOFs; (b) XPS to examine the oxidation state of MNPs; (c) HRTEM, STEM, PXRD, and EDX to ensure the size and distribution of MNPs, and (d) a single crystal tilt experiment or tomographic reconstruction to locate the position of MNPs in the MOFs.[50]

After MNPs loading, significant amplification occurs in the catalytic efficiency of the produced nanocomposites. The size regime in the nanorange has high surface density and very dense uncoordinated sites. Further, in photocatalytic reactions, metal loading greatly supports visible light absorption using localized surface plasmon resonance (LSPR) upon exposure to visible light irradiation.

Pd@UiO-66(NH$_2$) was fabricated by the simple mixing of MOF, PdCl$_2$, NaI, and PVP in an autoclave, followed by heating. The introduction of Pd causes an increase in visible light absorption intensity for MOF. The prepared nanocomposites Pd@UiO-66(NH$_2$) displayed greater catalytic efficiency than bare MOF UiO-66(NH$_2$) during the reduction of Cr(VI) and photodegradation of dyes after visible light irradiation. The enhanced photoactivity of Pd@UiO-66(NH$_2$) is due to the

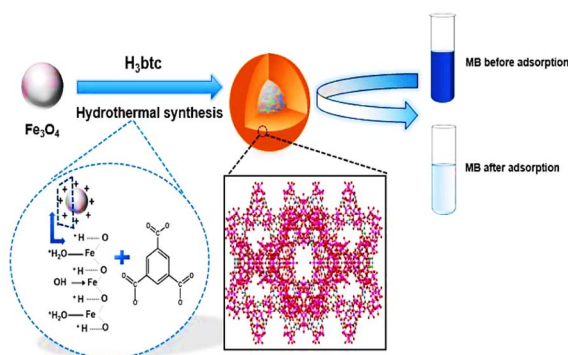Fig. 7 Schematic representation of the in situ one-step hydrothermal synthesis of Fe$_3$O$_4$@MIL-100(Fe) core–shell magnetic microspheres (reproduced with permission from ref. 45. Copyright 2017 Elsevier).

combined effect of the more efficient separation of the electron–hole pair and increased surface area. The Pd NPs take up the excited electrons from the MOF and hence reduce the Cr(VI) double solvent approach, followed by the encapsulation of Pd NPs in the pores of MOF.

Apart from photocatalysis, enzymatic activity-based applications also show better results in the case of such nanocomposites as compared to simple MOFs. Wang *et al.* used Pt NPs confinement in MOF Uio-66 with a different weight percentage of Pt-entitled Pt/Uio-66-1%, Pt/Uio-66-3%, and Pt/Uio-66-6% by varying amounts of K_2PtCl_4.[51] TEM, SEM, and PXRD ensured the successful insertion of Pt NPs into the pores of MOF along with the retention of the same crystal structure, as depicted in Fig. 8.

The embedment of Pt content in Uio-66 enhanced the enzymatic activity of Uio-66 in a specific trend as 6% Pt > 3% Pt > 1% Pt. Hence, the colorimetric sensor for the detection of glucose using the Pt/UiO-66 nanocomposite would not be able to sense as the zirconium-based MOF was unable to respond to enzymatic action.

2.3.2 Semiconductor embedding. Employing semiconductors of narrow band gap on MOFs is promising due to heterojunctions and hence the excellent activities of the produced nanocomposites. The same is caused due to enhanced separating tendency of photogenerated electrons and holes due to the process of electron transfer between the embedded semiconductors and MOFs. Semiconductors such as CdS, CdSe, Bi_2WO_6, BiOBr, and $BiMoO_6$ can be employed for the generation of such nanocomposites. CdS comes out as the best choice among the semiconductors because of its size-dependant optical and electronic properties along with a narrower band gap, *i.e.*, 2.4 eV. Moreover, many ternary nanocomposites, *i.e.*, the formation of the composite using three different components, have also been used in this field. Ternary composites are obtained after the addition of r-GO in the composites of MOFs, and semiconductors are also reported to show even better applications than binary nanocomposites. g-C_3N_4 nanosheets employed on MOF@MNPs also act as efficient ternary nanocomposites with appreciable activities. Graphite carbon nitride has aroused intensive interest toward this field due to its narrow band gap and conjugation (π–π).

Guo *et al.* prepared MOF nanocomposites with metal oxide semiconductor TiO_2 using a two-step process. The prepared photoanodes of NH_2-MIL-125/TiO_2 facilitated the transfer tendency of the electron–hole pairs along with the promotion and protection for photocathodic 304SS when irradiated under visible light. This TiO_2 nanotube-based heterojunction avoids the electron–hole pair recombination, proceeding further to achieve efficient photocathodic protection.[52] Zhao *et al.* devised a nanocomposite heterostructure using semiconductor nano-rods CdS and ZIFs that is capable of enhancing the current density of CdS with the simultaneous lowering of the HER overpotential. Further, a variety of heterojunctions with different doped metals were fabricated CdS–ZnM–ZIF (M = Cu, Ni, Co) to study photocatalytic hydrogen generation. The nanocomposites had the properties of inhibiting the recombination of charge carriers and hence promoting the transfer efficiency by separating the charges.[53] The effective energy transfer from a light-harvesting framework (IRMOF-3) enclosing each semiconductor quantum dot (QD) as a surface modification boosted their photoluminescence. The direct growth of IRMOF-3 crystals without any intermediary layer, such as polymers, on the QD surface is shown (Fig. 9).[54] Fluorescence lifetime measurement and steady-state excitation spectra measurement both supported the reported photoluminescence amplification caused by IRMOF-3's light harvesting.

2.3.3 Decoration by carbon materials. The addition of carbon materials in MOFs recombines the photoinduced charges and results in the acceleration of charge transfer. The coupling of MOFs with carbon materials further resolves the issues of fast recombination of charges in pristine MOFs. Various nanocomposites based on carbon dots and r-GOs have evolved as they have excellent electron conductivity, smooth
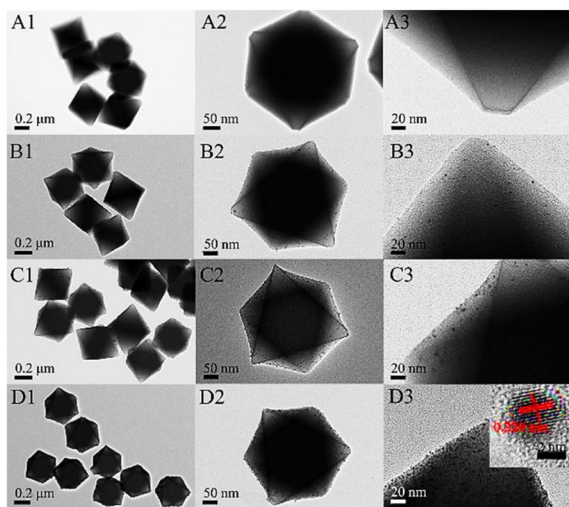
Fig. 8 TEM images at low and high magnifications of UiO-66 (A), Pt/UiO-66-1% (B), Pt/UiO-66-3% (C), and Pt/UiO-66-6% (D). The inset in (D3) is the HRTEM of the Pt particle (reproduced with permission from ref. 51. Licensed under Creative Commons Attribution 4.0 International License (https://creativecommons.org/licenses/by-nc-nd/4.0/) © 2021 ACS Omega).

Fig. 9 Schematic illustration for the QD based surface modification of IRMOF-3 (reproduced with permission from ref. 54. Licensed under Creative Commons Attribution 4.0 International License (https://creativecommons.org/licenses/by-nc-nd/4.0/) © 2021 ACS).

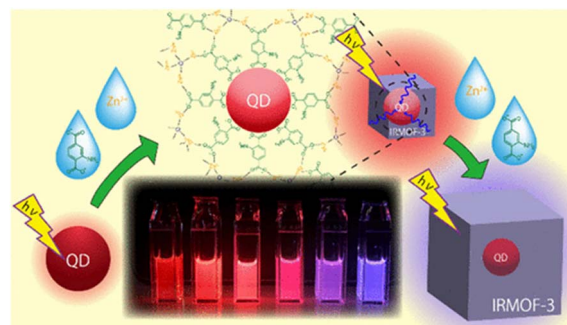functionalization, cost-effectiveness, and low toxicity. Noor et al. synthesized five r-GO@NiO-MOF nanocomposites in 1–5% wt r-GO. The successful incorporation of r-GO within the wrinkled nanosheets of MOF was confirmed by SEM and PXRD analysis. r-GO@NiO-MOF showed an enhancement in the catalytic activity for the methanol oxidation reaction. This intensification in the efficiency of nanocomposite is due to the involvement of the synergic nature of NiO-MOF and r-GO sheets. The process of methanol oxidation requires the smooth adsorption of methanol first and then its oxidation. The surface area of r-GO sheets and the porosity of MOF promotes methanol adsorption in the MOF voids in an enhanced manner due to the assistance of r-GO. The prepared nanocomposite displayed an appreciable tendency for the generation of hydrogen by methanol oxidation. The r-GO (5%)/NiO-MOF nanocomposite gave exceptional applicability with a low potential value (0.8 V) and lowest impedance and highest peak current density (275.85 mA cm^{-2}). Hence, these materials provide an alternative efficient way to improve the properties of MOFs, maintaining the same crystal structure and morphologies.[55]

Similarly, Akbarzadeh et al. synthesized the nanocomposite Ag$_3$O$_4$/r-GO-/Cu-MOF, which successfully degraded AB92 dye with improved efficiency. The improved activity of the nanocomposite was due to its increased surface area, efficient separation, and transport of charge carriers. The surface area calculated from BET was about 5.63 m^2 g^{-1}.[56] Nanocrystals of a Co-based MOF, ZIF-67, were synthesized by Xia et al. Further, after pyrolyzing the produce, nitrogen-doped carbon nanopolyhedrons were fabricated.

The carbonized MOF NPs were found to show ORR (oxygen reduction reaction) activity similar to the Pt/C catalyst. Zou and co-workers studied the effect of particle size of nanoMOF and the corresponding derived material on the catalytic activity. They synthesized ZIF-67 in various conditions to achieve different particle sizes ranging from bulk to 300 nm. The polyhedral morphology of the MOF nanoparticles was retained in the MOF-derived carbon materials (MDCs) by carefully choosing the pyrolysis temperature under Ar atmosphere, which is ascertained from TEM. The synthesized carbonized MOF NPs have a BET surface area of 386 m^2 g^{-1}. The ZIF NPs had narrower pore size distribution of 0.9 nm, while after carbonization, mesopores in the range of 2–5 nm and pores with a size greater than 26 nm were formed. This study put forward a small particle size having more exposed and easily accessible active sites for a fast electron transfer process.[57]

Moreover, nowadays, MOF-derived carbon-based nanocomposites are also captivating the attention of researchers. The innovative porous Fe$_3$O$_4$@NPC composites were successfully created by in situ formation during the thermal breakdown process utilizing Fe-MOFs as the template material.[58] The Fe$_3$O$_4$@NPC composites, which were made up of Fe$_3$O$_4$ nanoparticles uniformly scattered in the ordered octahedral structure of the carbon matrix, preserved the original octahedral appearance (Fig. 10). The well-designed structure of the Fe$_3$O$_4$@NPC composites and the synergistic interaction between Fe$_3$O$_4$@NPs and NPC were credited with the
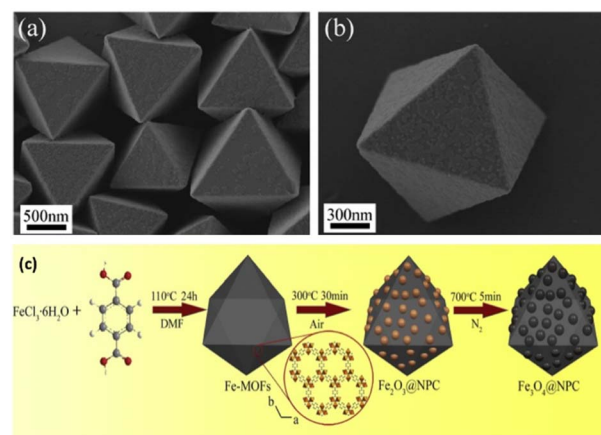

Fig. 10 SEM images of (a) Fe-MOF crystals, (b) single Fe-MOF crystal, (c) schematic representation for the synthesis of nanocomposite Fe$_3$O$_4$@NPC derived from Fe-MOF. Reproduced with permission from ref. 58. Copyright 2019 Springer.

exceptional performance. As a result, this work may offer a fresh perspective on the design and synthesis of materials that may effectively block electromagnetic waves.

3. Applications of NMOF nanomaterials

3.1. Catalysis

MOF nanomaterials have a wide range of applications. One of them is catalysis. NanoMOFs can act as efficient water/oxygen oxidizing catalysts (WOC). For example, Wang et al. described the potential of nanocrystalline Co–ZIF-9 nanomaterial as an effective water oxidation catalyst.

Nanomaterials derived from MOF have prominently been used as an excellent catalyst in the adaptable catalytic process for the elimination of contaminants. MOF derivatives have a great potential for active site exposure due to their large surface areas. After the formation of nanocomposites of MOF, the retained morphology and variable pore size both help in improving the performance of the catalyst.[59] Because of these advantages, compounds derived from MOF are suitable candidates for a catalytic reaction that occurs in the environment. We mainly focus on three processes: (1) photocatalysis, (2) Fenton-like catalysis, (3) persulfate (PS)/peroxymonosulfate (PMS)-activated catalysis.

3.1.1 Photocatalysis. In the last few years, nanocomposites derived from MOFs have been actively used as heterogeneous catalysts, which exhibit favorable activity in photocatalysis. Regardless of their composition or structure, these hybrids have strong competitive advantages over conventional photocatalysts. In particular, MOFs with multiple centers can directly transform into semiconductors such as metal sulphides and metal oxides. Furthermore, derivatives from doped heteroatoms can be obtained from organic linkers without additional additives. Regarding their structure, pronounced morphology and ultrahigh porosity accelerate the contact between the reactants

and charge carriers, thus effectively confining the recombination of photogenerated electron–hole pairs. In UV light irradiation, excitation occurs from the photons in the CB and VB, respectively [CB = conduction band, VB = valence band].

With regards to physical science (thermodynamics), the light-generated species (holes/electrons) may scale back O_2^-, and holes, which are left in the valence band, will react with OH^- to generate the hydroxide radical ($OH^{\cdot}$).[60] On the other hand, the holes having a strong oxidative ability can directly bring about the light oxidation of chosen impurities. These extremely active species play a vital role in photocatalytic degradation. Numerous studies have demonstrated improvement in the electronic and optical properties of photocatalysts such as extending the lifetime of diving h^+/e^- pairs, intensifying the photoharvesting power, and promoting the conduction of charge carriers.[61,62]

3.1.2 Photocatalytic reduction of CO_2.

Over the last few shift growth decades of human civilization, global warming has become an issue of great concern. Fossil fuels cannot be excluded while talking about global warming, and their over-consumption leads to the global energy crisis. During combustion, a lot of CO_2 is emitted, which leads to the greenhouse effect. The most useful method to solve this issue is the photocatalytic reduction of CO_2. This method not only acts as a remedy but instead can be regarded as a magnificent way to fabricate profitable chemical fuels that can be used in industries for a noble cause. MOFs having porous and crystalline properties can be used as catalysts for the photocatalytic reduction of CO_2 due to their distinct structure for extensive mechanism understanding.[63] Further, primarily two kinds of metal nanoparticles with well-defined functions have been introduced into MOFs. Those are catalytically active metal nanoparticles and plasmonic metal nanoparticles. Plasmonic metal nanoparticles have general cases of Ag, Al, and Au nanoparticles that can be introduced to improve the light absorption ability of the photocatalyst and infusion of hot electrons.[64,65] On the other hand, catalytically active nanoparticles such as Au@Pd, Pt, and Au@PtHg can be introduced for the trapping and photogeneration of electrons for photocatalysis.[66]

3.1.3 Photodegradation of contaminants.

Environmental pollution is a great concern in the 21st century. Heavy metal pollutants and organic pollutants have seriously jeopardized our human lives and limited our development. Among various methods, the photodegradation of pollutants has gained considerable attention among researchers as it is one of the methods that utilizes renewable solar energy. In addition, photocatalysts of metal nanoparticle/MOF composite have obtained great progress in this field of photodegradation of organic pollutants causing pollution.[67,68]

Wu et al. studied the performance of photodegradation of metals M (M = Au, Pd, and Pt)@MIL100(Fe) ($Fe_3O(H_2O)_2(OH)(BTC)_2 \cdot nH_2O$ ($n \approx 3.2$)) concerning organic contaminants.[69] These studies were done under visible light (≥ 420 nm) by the use of methyl orange as a dummy pollutant and oxidizer as H_2O_2. Expectedly, all the M@MIL-100(Fe) composites exclusively showed magnificent photodegradation activity as compared to crude MIL-100(Fe). The photocurrent and photoluminescence results showed that this enhancement is due to the addition of metal nanoparticles, which enhanced the charge transfer ability amidst M@MIL-100(Fe). In addition, among all the composites of M@MIL-100(Fe), Pt@MIL-100(Fe) showed the best photodegradation effect. This was validated through charge-carrier separation and visible light absorption data. The other upcoming pollution source is heavy metals, more seriously, through Cr(VI), which is discharged in large amounts from textile industries. Also, steel manufacturing causes a significant threat to the earth. Likewise, the nanoparticle-based MOF have shown significant charge carrier ability (Au@MIL-100(Fe) (0.1861 min^{-1}), Pt@MIL-100(Fe) (0.5618 min^{-1}), MIL-100(Fe) (0.1518 min^{-1}), Pd@MIL-100(Fe) (0.2883 min^{-1})). Moreover, Hu et al. also used Co–Fe bimetallic MOF-derived nanocomposite ($CoFe_2P@mC$) for the photocatalytic degradation of rhodamine B (Rh B) dye. The schematic representation is shown in Fig. 11. After the passage of 30 min, the nanocomposites achieved 99.7% degradation efficiency.[70]

3.1.4 Fenton-like degradation.

In the last few years, catalysis (Fenton-like) has been used as a preoxidation technology for decomposing stubborn organic pollutants in wastewater and is a subject of great interest. In this method, (Fenton-like) hydroxyl radicals prepared in situ are highly reactive species and major oxidants for organic pollutant degradation. In general, low-valent metal ions can operate H_2O_2 to decompose to generate OH radicals, which continuously decompose the target, then H_2O_2 reduces the high-valent ions to realize a redox cycle, ensuring that the catalytic reaction occurs before the reaction. Furthermore, the secondary metals present in the catalyst can induce the rapid conversion of two metal redox pairs as well as the catalytic decomposition of H_2O_2; thereby, the efficiency of the electrolytic system is increased.[71] After the introduction of optical radiation, the light-excited electron can do two things—generate OH radical by reaction with H_2O_2 as well as speed up the reuse of metal species.

The reaction between H_2O_2 (cathodically produced) and metal ions on the surface of the catalyst can yield reactive OH radicals in the electro-Fenton system.[72] The succeeding
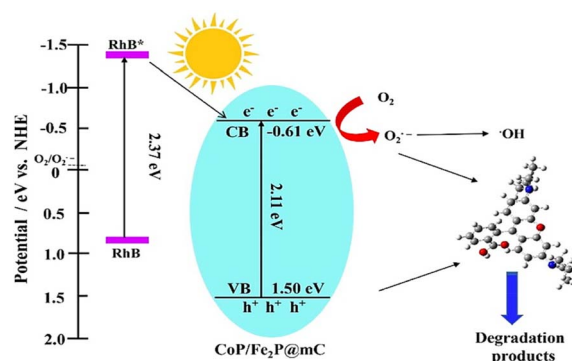

Fig. 11 Schematic illustration of the photodegradation process of RhB over the CoP/$Fe_2P@mC$ nanocomposites (reproduced with permission from ref. 70. Copyright 2018 Elsevier).

oxidation process can benefit from improved efficiency and lower costs associated with the consumption of H_2O_2 from such a reaction of H_2O_2 (generated *in situ*). In this area of research, nanomaterials derived from MO have permanent porosity, tailored texture, well-defined structure, and a huge surface area. This makes it possible to quickly develop heterogeneous catalysts for Fenton-like systems. The catalyst derived from transition metals such as Co, Cu, and Fe among the various derivative reported from MOFs, exhibit significant potential in Fenton-like heterogeneous systems.[73,74]

For the forward oxidation process, the synthesis of an efficient and recyclable catalyst of Fenton-like is still a crucial factor. By controlling the calcination of Fe-based MOF in 2 steps, Fe_3O_4/C with an octahedral shape was obtained. Interpreted nanoparticles of Fe_3O_4 covered with a carbon layer made of graphite provide an ample channel of solid–liquid in the mesopore, assembling the porous octahedral. Graphitic carbon's oxygen-containing functional group also give the catalyst its hydrophilic nature and ability to dissolve easily in water. For decaying the organic dye MB (methylene blue) with the assistance of H_2O_2, the Fe_3O_4/C porous octahedral demonstrates the efficient Fenton-like heterogeneous reaction and nearly 100% elimination efficiency in 1 h. In addition, a magnetic catalyst's ability to be separated by an external magnetic field maintains its activity after 10 cycles. This indicates the long-term durability and recyclability of the catalyst. The unique mesoporous structure derived from the MOF, in addition to the sacrificial role and stabilizing effect of the carbon layer made of graphite, is responsible for the excellent catalytic performance of Fenton-like synthesized octahedral Fe_3O_4/C. The structure with an integrated porous octahedral carbon layer made of graphite can be easily synthesized using this easy method, and the catalyst has noteworthy capability for the treatment of wastewater.

3.1.5 Persulfate (PS)/peroxymonosulfate (PMS)-activated catalysis. Currently, utilizing catalysts to initiate PS/PMS has been contemplated to remove contamination due to their high selectivity and great oxidation ability. In this process, MOF-derived nanocomponents with favorable compositional and structural properties are extensively utilized as emerging catalysts. The nonradical and radical pathways are involved in the potential mechanisms for PS/PMS activation of nanomaterials derived from MOF to remove organic contaminants. When it comes to metal oxides, radicals such as $OH^{\bullet}$ and $SO_4^{\bullet-}$ dominate the catalytic degradation process. During the oxidation process, the breaking of the –O–O– (peroxide bond) of PS/PMS can cause SO_4 to be produced, which breaks down and limits the decay or break down the molecules of pollutants into H_2O and CO_2, thus transforming the remaining molecules into intermediate molecules of small size.[75] Nonradical (primarily electron transfer) catalytic process can be prompt to operate PS/PMS and additionally break down organic pollutants concerning carbon materials and carbon/metal hybrids. By overcoming the inertness to chemicals of the sp^2 carbon (C) configuration, carbon's graphitic N atoms can cause electron transfer from the carbon atoms to the nearby graphitic nitrogen, resulting in positively charged reactive sites. Graphitization degree, *i.e.*, the degree to which carbon atoms form closely packed hexagonal graphitic structure, N doping of C (carbonaceous) catalyst, and conductivity are primarily responsible for the effectiveness of the oxidation process of nonradicals.[76]

Nevertheless, the pathway of nonradicals has not been fully revealed and further in-depth studies are required to clarify it. Catalysts of transition metal, especially the numerous metal oxides, have adaptable benefits. Being exceptionally redox reactive, ferromagnetic, and multifunctional (such as antibacterial and so on) materials, metal oxides are supposed to be the most powerful and effective catalysts for encouraging the activation of PS/PMS.[77,78] BPA (bisphenol A) is a chemical that is used extensively in bottles, plastics, packaging, epoxy resins, and paper. It is one of the common organic pollutants that is found in waste water. BPA, which is categorized as an EDA (endocrine-disrupting compound), is detrimental to the growth of reproductive organs. The secondary waste, slow process, high cost, *etc.*, and other drawbacks of traditional treatment such as adsorption, biological treatment, and photocatalytic treatment typically limit their application. As a result, productive methods for removing BPA (bisphenol A) from the contaminated environment must be developed immediately. As a result, a straightforward strategy was developed by pyrolyzing the precursors of predesigned FeyCo1 y-Co nanospheres of PBA for the removal of BPA with the help of activation of PMS. Li *et al.*, for instance, demonstrated porous, hollow nanocages of Fe_x-$Co_{3x}O_4$. By activating peroxymonosulfate (PMS), the elimination mechanism of bisphenol A (BPA) from water and the catalytic performance of the nanocages was thoroughly examined. The catalytic stability and the effect of various process parameters on the efficiency of BPA degradation were investigated. The final morphology of $Fe_xCo_{3x}O_4$ was found to be significantly influenced by the amount of Fe doping. As the amount of Fe increased, the shape became moderately more consistent and the size of the particle increased to 160 nm from approximately 80 nm. It is clear from the results that porous nanocages of $Fe_xCo_{3x}O_4$ can work as different beneficial catalysts for the removal of pollutants by PMS activation.[79]

Researchers have developed these MOF-based catalysts to great benefit in polymerization operations. Owing to the advantages of their intrinsic porosity and synthetic abilities to build structurally well-defined single-site catalysts, MOF-based catalysis is becoming popular. More specifically, MOFs have been developed and tested for a wide range of heterogeneous catalytic reactions, including alcohol oxidation, ozone decomposition, detoxification of chemical warfare agents, and olefin oligomerization.[80,81]

3.2. Sensing

The majority of commercially available sensors use organic or inorganic polymers as active components that can react with or absorb the desired analyte.[82] For a sensor to function well, the electrical or mechanical qualities of these materials are important. The concentration of analytes, various physical and chemical properties of the analytes, and the active materials, including acidity or basicity, electron accepting–donating
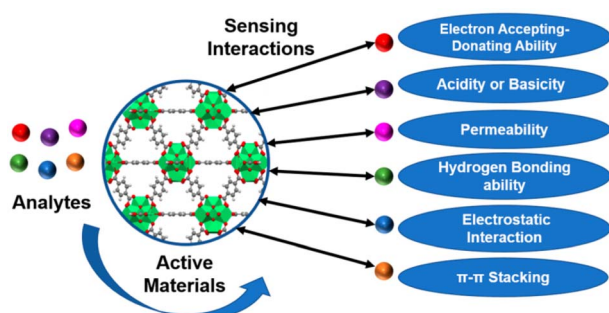
Fig. 12 The schematic diagram for the various interactions involved during the sensing of analytes (reproduced with permission from ref. 83. Copyright 2021 Chemosensors).

ability, hydrogen bonding capability, permeability, electrostatic interaction, and π–π stacking, all influence the degree of changes (Fig. 12).[83]

MOF nanostructures hold remarkable properties such as large surface area, tunable size having porous and active sites, and high chemical and thermal stability. Their most common applications are in adsorption, storage, catalysis, and sensing. Their features make them capable of the selective trapping and detection of various analytes from aqueous samples. Further advancements are achieved by modifications through the formation of nanocomposites of composites and their performance in electrochemical and luminescent-based detection performances.[84] MOF nanostructures have vast sensing abilities including the detection of luminescent sensors, electrochemical sensors, gas sensors, and colorimetric sensors. Gumilar et al. outlined a basic method for creating hierarchical three-dimensional M-BDC (M = Cu, Mn, Ni, and Zr) MOFs that are constructed from two-dimensional nanosheets or nanoplates in the presence of acetonitrile and PVP as shape-directing substances.[85] The production of the hierarchical sheet- or plate-like M-BDC MOFs is highly influenced by the mass ratio of the precursor metal to PVP and the quantity of acetonitrile (Fig. 13).
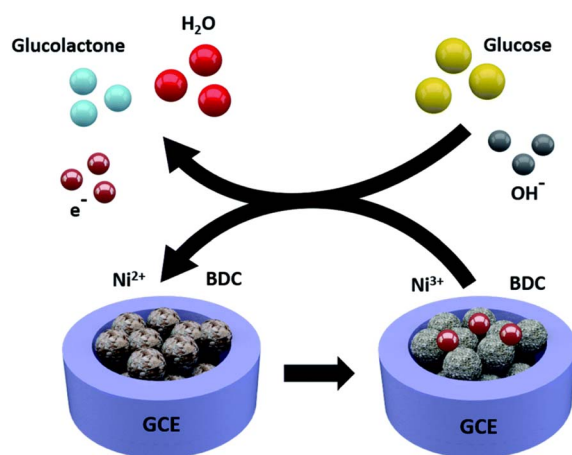

Fig. 13 Electrochemical glucose sensing mechanism for the Ni-BDC sensor (reproduced with permission from ref. 85. Copyright 2020 RSC).

While PVP aids in the nucleation and development of the MOF crystals. Acetonitrile maintains the solvation of the metal precursor. Bulk MOF crystals are produced when acetonitrile or PVP is removed. Only the hierarchical sheet-like electrode of Ni-BDC exhibits a significant amperometric response for glucose when used for nonenzymatic electrochemical glucose sensing. It has a high sensitivity of 635.9 μA mM^{-1} cm^{-2} and a broad linear range between 0.01 and 0.8 mM. The hierarchical sheet-like Ni-BDC electrode's detection limit for glucose is approximately 6.68 μM. This work is anticipated to offer practical methods for the future synthesis of hierarchical 3D MOFs and to encourage the direct application of MOFs in additional electrochemical applications.

The number of sensors based on MNPs/MOFs composites has dramatically expanded during the past years. The use of MNPs/MOFs composites in various sensing applications and how they work in concert to enhance the sensing display are briefly discussed. Then, they are classified into several sensors involving electrochemical sensing, fluorescence sensing, colorimetric sensing, SERS sensing, and CL/ECL sensing, which are introduced with special emphasis, in accordance with the types of sensors based on MNPs/MOFs composites.[86] The traits of MNPs and MOFs in particular, which have synergistic processes and are frequently used to categorize the reciprocal effects of MNPs and MOFs, are reviewed as follows. (1) MNPs perform the role of active centers, whereas MOFs stabilize MNPs. (2) To ensure signal confidence, MOFs restrict easily aggregable MNPs. (3) Because MOFs have significant porosity, it is feasible to guarantee the admission of reactants of the right size, which then react with the MNPs as active centers. (4) Active sites for simultaneous catalysis can be either MNPs or MOFs. These sensors can further selectively detect inorganic metal ions, heavy metal ions, volatile organic compounds (VOCs), and persistent organic pollutants (POPs) from the environment to decontaminate and provide favorable surroundings for global existence.

3.2.1 VOCs sensing. Various harmful gases present in the ecosystem are comprised of an array termed VOCs, which are detrimental to human beings, plants, as well as animals by polluting the environment in which they survive. VOCs contribute to environmental degradation primarily by destroying the ozone layer and introducing uncertainty in climate change.[87] Breathing, a crucial process for living beings, is also a constant emission source of VOCs. Thus, to live in a healthy environment, there is a critical need to remove VOCs.[88]

The outstanding structural flexibility and selective host–guest response fabrication of MOFs-based chemical sensors have captivated researchers for the removal of VOCs. In MEMS-based sensors, after the nanoparticulation of MOFs, there occurs a simple and effective deposition of MOF NPs as the receptor layer. Moreover, the mechanical stability of multiple coatings of MOF NPs is enhanced after the size reduction of MOFs to MOF NPs due to multiple MOF NPs coatings.[89]

The fabrication of a capacitive sensor for VOCs based on the nanoparticles of MOF (Cu-BTC) was done by Homayoonnia et al. Various concentrations of methanol, isopropanol, ethanol, and acetone were detected by the capacitive sensor having films of

MOF NPs, i.e., Cu-BTC NPs as the dielectric layer. Gas molecules, upon adsorbing into the pores of Cu-BTC NPs, produced a change in the capacitance value. The capacitance change after the interaction of analytes is attributed to a change in the dielectric constant of the material, i.e., Cu-BTC NPs [eqn (1)].

$$C = (\varepsilon_0 \varepsilon_r A)/D \qquad (1)$$

Then, measurements were taken for the change in capacitance. The sensor proved high selectivity to polar analytes with a sensitivity value of 250–1500 ppm. In addition, the sensor possessed good response time and excellent linearity.[87] Yeung et al. evidenced new advancements in the family of microelectromechanical sensors, i.e., MEMS by devising novel MOF-MSS sensors based on the ZIF-based family of MOFs. A suspension of four different MOF NPs derived from ZIF-7, ZIF-8, ZIF-65, and ZIF-71 was deposited on the MSS membrane via spray coating. The efficacy of these sensors can be understood by their unparalleled response time, i.e., 1–30 s and sub-ppm sensitivity range for the clear differentiation and selective determination of VOCs. A wide range of vapors from 26 VOCs containing various classes such as water, alcohol, ketone, carboxylic acid, amide, and ester was used for the study.[89] Cao et al. further described the mechanistic path for the sensing of acetone using $ZnFe_2O_4$/Fe–ZnO nanocomposite with a response of 30.8–100 ppm, as shown in Fig. 14.[90]
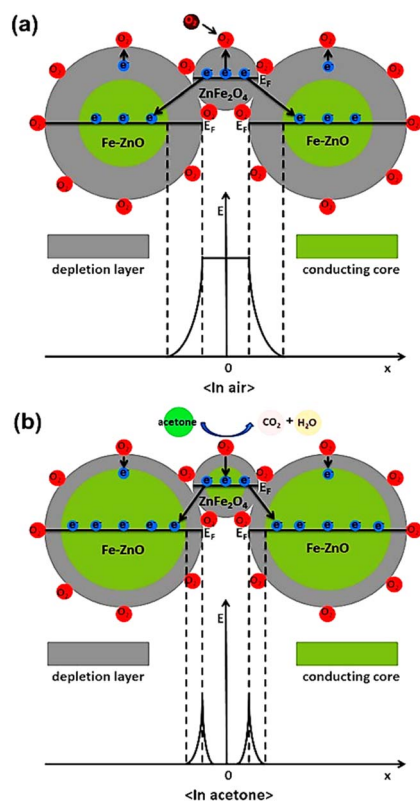

Fig. 14 Schematic diagram of the structure and band for the $ZnFe_2O_4$/Fe–ZnO nanocomposite-based sensor (a) in air and (b) in acetone (reproduced with permission from ref. 90. Copyright 2020 Elsevier).

Li et al. discussed some of the most recent developments in MOF sensing and switching materials with a focus on electrical, magnetic, ferroelectric, and chromoelectric sensing mechanisms.[91] It was done with a thorough examination of the MOF–analyte interactions in these procedures, which are crucial to the sensing effectiveness of MOF-based sensors and switches.[92,93] The authors have described in great detail the potential uses of MOF-based sensing and switching materials for the detection of water vapor, oxygen, toxic industrial gases (such as ammonia, hydrogen sulphide, nitrous oxide, sulphur dioxide, carbon oxides, and carbon disulfide), and VOCs (such as aliphatic and aromatic hydrocarbons, ketones, aldehydes, alcohols, chlorinated hydrocarbons, and N,N-dimethylformamide).[94]

3.2.2 POPs sensing. The increasing number of organic pollutants including antibiotics and pesticides are rapidly becoming of great concern for the health of our ecosystem. Despite antibiotics being a necessity as medicine for bacterial infections, their residual material poses a great problem toward human health and the environment. On the other hand, pesticides have agricultural benefits but their residues are very challenging to degrade. The persistence of such organic pollutants may cause serious ailments such as neurotoxicity or may lead to breast cancer, brain cancer, and even sexual disorders. Hence, to put a check on such POPs, there is an urgent requirement to detect such pollutants in environmental samples. The nanostructure of MOFs is promising for performing this desired task due to their compatible features such as high surface area, porous nature, linking abilities, and high catalytic abilities.[95]

Zirconium-based MOF nanostructures provide vast applications in the field of pesticide detection. Yang et al. employed a nanocomposite Fe_3O_4@SiO_2@UiO-67 based on Zr-MOF for the selective detection of glyphosate. The prepared nanocomposite displays a selective feature due to its Zr–OH group that has a high affinity to the phosphate groups. In addition, an alteration in the fluorescence intensity of the nanocomposite occurs after interaction with the pesticide glyphosate. Silica incorporation retards electron transfer between the magnetic core of Fe_3O_4 and UiO-67, hence making the identification of glyphosate possible along with its concentration. The sensor was found to have very high sensitivity (detection limit = 0.093 mg L^{-1}), high absorptivity (256.54 mg g^{-1}), and excellent reusability.[96]

Similarly, the work of Li Ma et al. on the nanocomposite formed with the anchoring of Pt NPs over UiO66-NH_2 provided acetylcholinesterase (AChE) biosensors for malathion, as depicted in Fig. 15. Due to the increased surface area and electron conductive channels, there was an enhancement in AChE immobilization. The sensor was found to have a good detection limit for malathion. Moreover, Pt@UiO-66-NH_2@GCE was employed to successfully detect malathion in apple and cabbage samples.[97]

Li et al. have marked a milestone in this field by devising an immobilization-free and degradable sensor based on zeolitic imidazole framework-8 (ZIF-8) as a degradable carrier for methylene blue (MB) dye. The principle behind this sensor was
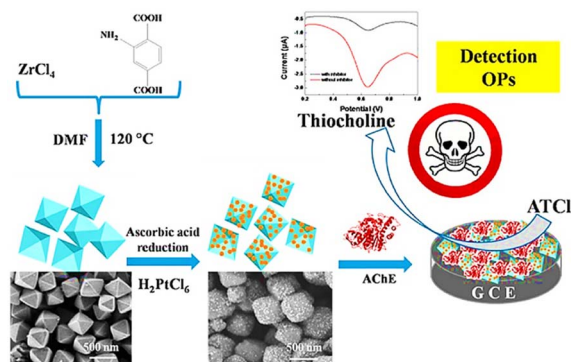
Fig. 15 Schematic representation of detection of organophosphates using Pt@UiO-66-NH₂@GCE (reproduced with permission from Li Ma et al.[97] Copyright 2019 Elsevier).

the AChE-catalyzed hydrolytic reaction that occurred after the dissolution of ZIF-8/MB nanoparticles under acidic conditions. The release of many MB molecules takes place to generate a strong diffusion current. Hence, AChE inhibitors were monitored by a decline in the electrochemical signals. The sensor based on the nanostructure of ZIF-8 displayed good analytical performance for paraoxon with a detection limit of 1.7 ng mL^{-1}.[98]

To put a check over environmental decontamination, Niazipour et al. put forward a 3D MOF (MOF-199) to detect antibiotics including azithromycin, amoxicillin, cefixime, ciprofloxacin, and gentamicin. The limit of detection was in the range from 0.14 to 0.62 μg L^{-1} in environmental and urine samples. Highly porous Cu nanofoam fibers were used to synthesize MOF-199 nanostructures for the solid-phase micro-extraction of antibiotics.[99]

In the literature, several applications of MOF-based materials have been shown for the sensing of nitroaromatics and pesticide as well.[100,101] MOFs made from metals such as zirconium, cerium, and hafnium, which are in group IV of the periodic table, have drawn great attention because they operate in watery media and have noteworthy chemical stability in water. Since 2013, numerous research publications on related MOFs for chemosensors have been released.[82] The functionality of chemoresistive sensors will also be improved by the addition of MOFs to a composite of active sensing materials. To prepare various electrically conductive MOFs and materials made from MOFs for use in a variety of applications, including chemoresistive sensors, numerous research activities have been carried out.[102] For instance, UiO-66 and its derivatives can be used to prepare chemically resistive sensors for the detection of CO_2, NO_2, and SO_2 gases.

3.2.3 Heavy metal ion sensing. Heavy metal discharge from industrial, domestic, and agricultural fields in water and environmental samples is a menace to health. Heavy metals are nondegradable and can exist in the form of ions, elements, and complexes. Some heavy metal ions are essential trace elements but are toxic at high concentrations, e.g., Zn^{2+}, Fe^{2+}, Mn^{2+}, and Cu^{2+}, while some are toxic at very low concentrations as well, e.g., Cd^{2+}, Hg^{2+}, As^{3+}, and Pb^{2+}. These ions have various

detrimental impacts including damage to the lungs, high blood pressure, vomiting, nausea, and neurotoxicity due to their certain features including aggregation in the body, excellent miscibility with water, and binding capacity with DNA and cell proteins. The binding interactions further lead to altering the protein conformations, which may prove to be carcinogenic.[103]

Various optical, biological, and electrochemical sensors have been developed for the successful detection of heavy metal ions. For the facile detection of such heavy metal ions, nanostructures of MOFs can provide a milestone as they are easy to incorporate and provide more surface area, more binding abilities, and easily approachable charge transfer processes.

Subsequently, due to certain excellent characteristics, MOF nanocomposites help in boosting the sensing mechanism. The porous structure accompanying the luminescent and magnetic properties of MOFs makes them a suitable material for adsorption and hence a selective sensing material.

Luminescence-based detection of Hg^{2+} ions was done by Xu et al. using an aluminium-based MOF (MOF-253) nanoparticle composite. Loading of MOF-253 was done with luminescent ion Eu^{3+} and optically active carbon dots (CD), resulting in the formation of the sensor Eu^{3+}/CD@MOF-253. The detection was based on the quenching ability of Hg^{2+} ions for the blue CD-based fluorescence without altering Eu^{3+}-produced red luminescence. The method displayed excellent sensitivity with an LOD value of 13 ppb.[11] Similarly, Liu et al. detected Cu^{2+} ions using four different MOF nanocages-based luminescent Ln-MOFs, 1-Ln (Ln = Eu, Tb, Gd, Dy). 1-Eu was found to have the highest selectivity and sensitivity for Cu^{2+} ions due to weak interactions between Cu^{2+} and the pyridyl sites. The synthesized compound also captured CO_2 gas selectively.[104]

An electrochemical sensor that selectively and sensitively enhanced the detection of multiple heavy metals (Cu^{2+}, Cd^{2+}, Pb^{2+}, Hg^{2+}) was reported by Wang et al. The sulfur-containing nanocapsule-based MOF sensor [Co-TMC4R-BDC] has a bowl-shaped cavity comprised of every nanocapsule unit (TMC4R = tetra(4-mercaptopyridine)calix[4]resorcinarene). The edges of the octahedron were occupied by eight equally distributed sulfur atoms, which efficiently trapped heavy metal ions. The reason for trapping was the stronger binding efficiency between sulfur and ions along with the existence of cation–π bonding between the phenyl ring and heavy metal ions. Further, a glass carbon electrode was employed to form Co-TMC4R-BDC/GCE for the simultaneous and individual detection for all four ions, which showed high sensitivity and low LOD value.[105] A core/shell UiO-66-NH₂@PANI composite was successfully prepared using a straightforward hydrothermal method with PANI coatings.[106] The generated composite modified electrode was used for the detection of trace quantities of cadmium ions using differential pulse stripping voltammetry. The analysis of cadmium ions in actual samples served as a demonstration of the practical applicability. A consistently nanosized octahedron, MOF-199, was prepared, and it demonstrated outstanding Cr(vi)-triggered oxidoreductase catalytic capabilities.[107] Cr(vi) was present, and the chemosensor used this to activate the catalytic activity of MOF-199, which is similar to an oxidoreductase. TMB was used as the chromogenic substrate. The
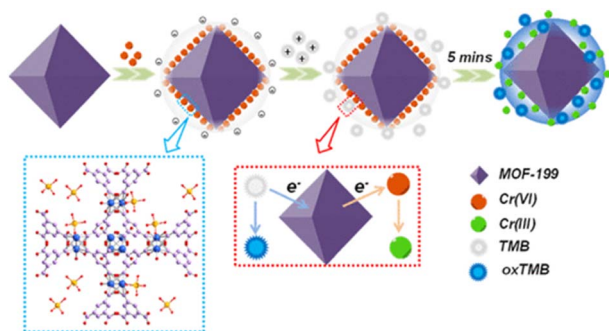
© 2023 The Author(s). Published by the Royal Society of Chemistry

Fig. 16 Schematic representation for the Cr(VI) sensing using nanozyme MOF-199 (reproduced with permission from ref. 107. Copyright 2021 ACS).

mechanistic pathway for the sensing is shown in Fig. 16. The nanozyme's steady-state kinetics was studied for the activity of the imitating enzyme. The concept of nanoscale MOF-based artificial catalysts with enzyme-mimicking activity can also be expanded in the future to monitor and detect other important compounds.

Wang *et al.* devised a highly sensitive colorimetric sensor (AuNP@MOF) comprising Au NP anchored in iron-porphyrin base MOF Fe-TCPP-MOF for the selective detection of Hg^{2+} ions. Hg^{2+} ion triggered the catalysis process to reduce methylene blue (MB) dye and thereby was sensed. Upon the introduction of the sensor into the sample, the Hg^{2+} ion was linked with the AuNPs surface and forms a gold amalgam. The gold amalgam formed to act as a catalyst for MB reduction. The sensor showed high sensitivity with an LOD of 103 pM and a response time of 2 s.[108] The work by Bhattacharjee *et al.* offers fresh perspectives on constructing selective and sensitive MOF-based sensors for nitroaromatics, such as explosive detection. A novel mixed-ligand Ni-MOF performing "turn-off" detection of trinitrophenol (TNP) from a purely aqueous medium was devised.[109] The synthesized MOF has good sensitivity (LOD = 87 ppb) and significant quenching efficacy by the combinatorial effects of RET, ICT, PET, and interactions as well as competitive absorption processes. In addition, the MOF-based chemosensor's quick reaction (5 s), recyclable nature, and accurate recovery of TNP in environmental water samples indicate its dependability and applicability.

3.3 Adsorption

The phenomenon of a solid substance's surface absorbing molecules or ions from the surrounding gas or liquid is known as adsorption. It has been extensively utilized in environmental fields such as heavy metal ion adsorption, PPCPs, and wastewater treatment due to its simple operation and low cost.[110,111] Traditional adsorbents (such as zeolite and silica) are currently experiencing difficulties such as a steady rate of rate and little capacity for adsorption.[112,113] One of the best adsorbents for water are COFs and POPs because of their extremely high Hg(II) adsorption capacity, quick adsorption kinetics, and high recycling efficiency. Hg(II) adsorptive removal using the nanoscale

porosity of organic polymers (mesoporous POPs, microporous POPs, COFs) has been reported.[114] DMTZ-PMO (a mesoporous silica-based porous material) containing thiol and thiadiazole moieties have also been used for the adsorption-based removal of toxic Hg(II) ions.[115] The mesoporous walls' covalently-bonded organic activity serves as a Hg(II) scavenger, and the material's stiff structure offers it stability to work well as an adsorbent throughout a wide range of pH, solvent, and temperature. The material is an effective adsorbent for Hg(II) removal because soft centers, such as sulphur, increase the mercury ion adsorption through soft–soft interactions. Despite their impressive benefits, porous organic nanoparticles are typically functionalized with phosphorus and sulphur-containing groups for effective interaction with mercury, which is dangerous to the environment. Therefore, for environmental concerns, mercury uptake with these nanoporous polymers is unacceptable. In the same context, owing to their ample pore sizes and highly determined surface area, carbon-derived MOFs have emerged as competitive adsorbents.[116]

Chemical oxidation, membrane technology, adsorption, and coagulation–flocculation are some of the technologies that have emerged for controlling wastewater pollution. Numerous efforts have been made to get rid of pollutants in the environment from water.[117,118] Due to the comprehensive consideration of cost reduction, procedure simplification, removal efficiency, and operational feasibility, the method of adsorption is a preferred option. As a novel type of adsorbent, nanomaterials derived from MOF are dominant in this process. In addition, scalable fabrication allows production at the industrial level more options.

Noticeably, knowing the mechanism of adsorption is important for more than just knowing the basics of adsorption; it is also important for improving the adsorption technology and developing it further for commercialization. The adsorbents' porosity and surface area typically have an impact on the adsorption capacity through van der Waals interaction. The syntheses conditions have an impact on the structural properties of MOFs that are produced through organic ligands and the coordination of metal ions. The synthesis of MOFs is generally influenced by several parameters, including the ligand, solvent, additive, duration, functional group, and metal source. Porosity, crystal size, morphology, MOF yield, and crystallinity are all affected by these parameters.

3.3.1 Heavy metal ion adsorption. The process of retaining and attracting particles or molecules on a solid material's surface is known as adsorption. MOFs have attracted great attention in recent years because they have a large surface area, pore sizes that can be changed, and a variety of uses. They have been widely researched for their possible applications in gas capacity, partition, catalysis, and medication conveyance. The fundamental elements of an adsorption cycle are energy, thermodynamics, stability adsorption limit/proficiency, selectivity toward adsorbate particles, and reusability or recovery. MOFs have excellent characteristics of MOFs, such as extremely high porosity, a tunable structure, a huge specific surface area (SSA) (Langmuir's SSA exceeded 6550 m^2 g^{-1}), and simplicity of preparation.[119] MOF composites are of keen interest because

they not only possess elevated water stability but also there is favorable kinetics and/or high adsorption capacity. Carbon nanotubes/MOFs (CNT/MOFs), graphene oxide/MOFs (GO/MOFs), and polydimethylsiloxane/MOFs (PDMS/MOFs) are some typical examples.[120,121] Furthermore, it is important to know the interaction mechanisms involved in the process of adsorption to develop a material with high adsorption performance. It is also known that the adsorption mechanisms of organic pollutants over MOFS primarily included hydrophobic, electrostatic, hydrogen bonding, metal bridging, and acid–base interactions.[122] To remove heavy metal ions from contaminated water, MOFs have appeared as promising alternatives. Due to their best absorption efficiency for the removal of heavy metal from contaminated water, MOFs have been utilized to remove heavy metal ions from contaminated water.[123] Because of their large surface area, pore geometry, and high porosity, MOFs are utilized in the adsorption process to eliminate poisonous substances from the environment.[124,125] MOFs have been used in gas storage and separation, photocatalysis, biomedical, and chemical sensing,[126,127] and they contain a variety of metals, including zirconium, aluminium, and chromium, all of which have been studied as effective adsorbents for the elimination of organic and inorganic contaminants from water. The porous structure of MOFs assists in the dispersion of pollutants to their active sites, resulting in faster consumption of the functional group and a simpler regulation of adsorption. The MOF node uses a pseudo-ion exchange method to remove even anionic pollutants, which are inorganic. This method easily binds organic ligands, which are then replaced by the next contaminant. The MOFs structure increases the adsorption capacity. For instance, the ZIF-8 has an exceptional highest adsorption capacity of 50 mg g^{-1} when it comes to removing As(v) from water, which is significantly higher than the adsorption capacities of activated carbon, which is 3 mg g^{-1}, and zeolite, which is 13.92 mg g^{-1}.[128] Recently, the adsorption of lead has become really popular. Saleem et al. examined the adsorption capacity of Zr-based UiO66NHC(S)NHME MOFs to decontaminate Pb^{2+} from water.[129] They discovered that the MOF has remarkable adsorption capacity, and the maximum adsorption achieved is 232 mg g^{-1}. Heavy metal removal from water by the MOF takes place by physical or chemical adsorption depending on the type of interaction between the adsorbents (MOFs) and adsorbates (heavy metal). Physical adsorption is also called adsorptive adsorption, whereas chemical adsorption is typically referred to as reactive adsorption. The strength of physical and chemical adsorption influences the adsorptive limit of MOFs. MOFs are crystalline materials made up of metal clusters or ions and organic linkers. The structure and properties of these materials can be easily changed by adding the right metal clusters or ions and organic linkers. In addition, a wide variety of MOF moderation is already known and utilized in synthetic and post-synthetic moderations.[130] Materials resembling graphene (such as diminished graphene oxide (GO)) appear to be among the best contenders for the improvement of MOF-based composites because of numerous significant benefits of GO such as high heat and electrical conductivity, chemical stability, and its feasibility for an extensive variety of modifications.[131]

The analytical performance of toxic metals with MOFs in food and water samples will be evaluated. There are various metal ions, e.g., Cd^{2+}, Pb^{2+}, Hg^{2+}, Zn^{2+}, and Cr^{3+}, reported as analytes for this process, but herein, we have explained the examples of lead and mercury.

The Cu-based MOF with an –SH group for rice and tea matrices has the best adsorption capacity and preconcentration factor (($SHeFe_3O_4/Cu_3(BTC)_2$) and ($CS/Cu_3(BTC)_2$–SH)), respectively, of the MOF types used for analysis and remove lead from food matrices.[132,133] MIL-101(Cr)/Fe_3O_4@PTSC (Cr-based), which uses fish as a matrix, outperforms other copper-based MOFs in terms of performance. For lead analysis with high recovery in sediment matrices, Fe_3O_4–DHz/$Cu_3(BTC)_2$ and Fe_3O_4 pyridine/$Cu_3(BTC)_2$ MOFs are structures with excellent analytical performance.[134] These studies demonstrate that the effect of the matrix and the performance of the MOF structures that are functionalized with a variety of matrix with various properties and may be acceptable for analysis should be taken into consideration when selecting MOFs. In studies using MOFs for lead analysis in environmental and food samples, Cu-based MOFs have high absorption capacity, while Zr-based MOFs, due to their stable nature in water environments, perform better in aqueous matrices. In aqueous matrices, Zr-based MOFs are preferred more because of their stability in aqueous environments.

Zr-based MOFs are typically used in studies related to matrices of water, whereas Cu-based MOFs are usually adopted for the investigation of Hg using MOFs in foods. In the research conducted by Wu et al., the modification method of photosynthesis was utilized to boost the MOFs' adsorption capacity for heavy metal ions and the tea matrix.[135,136] The wastewater matrix had a greater adsorption capacity in the study than wastewater and tea matrices, but the tea matrix's adsorption capacity increased with increasing adsorption time. It has been resolved that the effect of matrix and adsorption time is significant in matrices such as the matrix of tea. Aqueous matrices highlight the significance of selecting the appropriate metal ion in MOF synthesis, where the analytes are not just ligands or functional groups.

In conclusion, in food Pb analysis, Cu-based MOFs are typically used, even though lead ions from water samples are typically removed by Zr-based MOFs. In Pb analysis, the utilization of MOFs based on copper and zirconium has numerous advantages. The functionalization of MOFs to improve their adsorption efficiency plays a significant role in the trace analysis of heavy metal ions because it tends to enlarge the capacity. Adsorbents known as MOFs have advantages in terms of sorption capacity and prefactor.

With the right source of metal ions and functionalization for the analysis of toxic metal and ligand, MOFs are appropriate for use in environmental and food samples as highly sensitive, preconcentrating, and selective adsorbents having good capacity of adsorption. As a result, MOFs are favorable adsorbents for the quick and effective extraction of metal ions (heavy) from complex samples for environmental pollution control and food safety.

3.3.2 Pharmaceuticals and personal care products (PPCPs).

MOFs and their nanodesigned materials can adsorb PPCPs with great efficiency. MOF-based nanodesigned materials have countless applications such as gas purification, gas separation, energy storage, and hence, environmental decontamination. Among all the eminent applications, the distinctive architecture, high adsorptive performance, and physiochemical properties of MOF nanoadsorbents are highly attractive in the field of environment decontamination. MOFs and their nanostructures can be considerably used for the removal of PPCPs from wastewater samples. PPCPs are nonbiodegradable, biologically active substances that are water-soluble.[137] When disposed, they find a way to freshwater bodies and gather in the bodies of marine organisms.[138] It is ascertained that in sewage, more than 80 kinds of PPCPs can be found. PPCPs lie in the range from ng L^{-1} to µg L^{-1} in different sewerage, which has been explained by several studies.[139] Aquatic organisms show extensive consumption of PPCPs. Sulphonamide and TC (tetracycline) are antibiotics with high consumption. In addition, they are extremely stable and can penetrate the environment easily.

Porous carbons made from the pyrolysis of a subtype of MOFs were used to clean PPCP-polluted water, which is activated by KOH, by metal azolate framework-6 (MAF-6). A record of commonly used PPCPs includes acidic ibuprofen, weakly-acidic TCS, diclofenac sodium, basic atenolol, and oxybenzone; the MAF-6-derived porous carbons could potentially adsorb them. Importantly, after solvent washing, the carbon acquired 1000 °C promoted recyclability and had exceptional adsorptive properties for ibuprofen and diclofenac.[140]

Due to their widespread use as antipyretics and analgesics, KTP and NAP are considered EP's [KTP = ketoprofen[2-(3-benzoylphenyl) propanoic acid]; NAP = naproxen[2-(6-methoxynaphthalen-2-yl) propanoic acid]]. Both drugs can be assimilated into the water system in a variety of ways.[4] MIL-101(Cr) and GnO [graphene oxide] were used to prepare highly effective and porous MOF composites for the removal of KTP and NAP from water media. MIL-101/GnO composites outperformed pristine MIL-101 when it came to the adsorption of the tested anti-inflammatory drugs (AIDs). When compared to pure MIL-101 and mercantile-activated carbon, GnO/MIL-101 (3.0%) exhibited a greater adsorption capacity for NAP of 1.4 and 2.1 times, respectively. In addition, the as-prepared composite was reconstructed without significant deterioration and could be used for numerous cycles of continuous adsorption. It is found that pharmaceutically active and complex anti-inflammatory nonsteroidal micropollutants adsorb well on wastewater, surface, and ground samples.

Lin et al. developed MOF-808, MOF-802, and UiO-66 Zr(iv)-based MOFs. These MOFs were found to have remarkable adsorption capacities, as shown in Fig. 17. Amodiaquine, a chloroquine analogue, is widely used to treat and prevent malaria and other conditions of arthritis. Consequently, it is frequently found in wastewater and drinking water.[141] Tella et al. made zinc-carboxylate MOFs that were used to break down amodiaquine in water media.[142] [Zn$_2$(fum)$_2$(bpy)] and
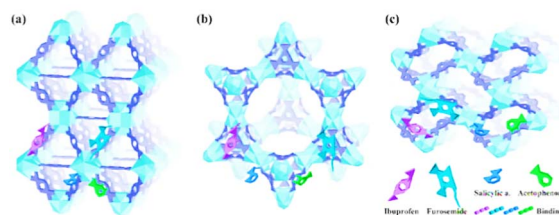

Fig. 17 Schematic diagrams of the interaction of ibuprofen, furosemide, salicylic acid, and acetophenone with UiO-66 (a), MOF-808 (b), and MOF-802 (c) (reproduced with permission from ref. 141. Copyright 2018 ACS).

[Zn$_4$O(bdc)$_3$] MOFs had adsorption capacities of 0.478 and 47.62 mg g^{-1}, respectively, for amodiaquine at an ideal pH = 4.3, according to the experimental profile. Five PPCPs were removed from the pristine and hydroxyl group of functionalized MIL-101s.[137] PPCPs include ketoprofen, BPA, TCS, NPX (anti-inflammatory and nonsteroidal drugs), and PCMX (p-chloro-m-xylenol), a bactericidal used in baby powders, deodorants, and creams because more hydrogen acceptor and donors are present.[143,144]

Due to their ease of fabrication, modification, ecosustainability, and convenient recovery, magnetic nanomaterials have attracted great attention these days. They also have important characteristics such as dispersibility, large surface area, and small size,[137] which allow these magnetic nanoparticles to be modified to achieve adsorption specificity and selectivity toward the target compounds.

3.3.3 Waste water effluent removal.

Adsorbents made of carbon nanomaterials derived from MOFs are widely used. Carbonaceous materials act as adsorbents due to their adjustable volume and uniform size distribution of pores, doping of heteroatom, and huge surface area. In the adsorptive process of removing four PPCPs, a bio-MOF-1-derived extremely permeable carbon was utilized.[145] The maximum acidic clofibric acid (CLAF) adsorption capacity (clofibric acid = 540 mg kg^{-1}) and basic atenolol (AATL) (atenolol = 552 mg g^{-1}) above BMDC-12 h were nearly two and ten times higher than those of the AC (commercial), respectively, making it a better adsorbent in comparison to previously reported ones. Electrostatic interaction can explain ATNL adsorption and H-bonding, in which CLAF and porous carbon act as H-donors and H-acceptors and dominate CLAF adsorption. Similarly, Ahmed et al.'s report on ZIF-8 materials derived from carbons (MDC1000) with BET surface area 1964 m^2 g^{-1} and pore volume 1.32 cm^3 g^{-1} were significantly higher than those of the parent MOFs and AC.[149] The maximum SMX adsorption capacities of MDC-1000 were 435 mg g^{-1}, nearly 20 times greater than the original MOF and four times greater than AC. Based on the interaction between the zeta potential of MDC and the pH of the solution, H-bonding can be used to reveal the mechanism of adsorption.

Due to the increased specific surface area and optimal porous structure, the pyrolysis of MOFs with additional carbon sources has the potential to significantly improve their adsorption capacity. For illustration, Xu et al. carbonized ZIF-8

Table 1 Classification of various MOF nanostructures on their applicability toward decontaminating environmental pollutants along with the specification of their corresponding MOF precursors and guest moieties

Sr. no.	MOF nano structures	Target pollutant	Mode of decontamination	Reference
1	$Fe-C_x$	Organic pollutant (4-nitrophenol)	Fenton-like catalytic degradation (catalyst amount = 0.08 g L^{-1}) (removal efficiency = 89% wt)	158
2	$CoP/Fe_2P@mC$	Dye (Rh B)	Photocatalytic degradation (catalyst = 100 mg L^{-1}) (removal efficiency = 94%)	70
3	$CoN/N-C@SiO_2$	Antibiotic (tetracycline)	PMS-activated catalytic degradation (removal efficiency = 98.7%)	159
4	α-Fe_2O_3/ZIF-67	Antibiotic (ciprofloxacin)	PMS-activated catalytic degradation (catalyst amount = 0.1 g L^{-1}) (removal efficiency = 99%)	160
5	$Pt@M-Cr_2O_3$	VOC (toluene)	Catalytic degradation (surface area = 77.4 m^2 g^{-1})	161
6	NiZn-MOF NSs	Organic pollutant (tyrosinase)	Sensing (LOD = 6.5 nM)	162
7	Co_3O_4-350	VOC (formaldehyde)	Sensing (LOD = 10 ppm)	163
8	(EuOF/quantum dots)	Trinitrotoluene (TNT)	Sensing (LOD = 3 ppb)	164
9	Co_3O_4@MOF-74	Fenamiphos insecticide	Sensing (LOD = 3 pM)	165
10	ZJU/GCE	Heavy metal ions (Cd^{2+} and Pb^{2+})	Sensing (LOD = 1.10 nM for Pb^{2+})	166
11	TiO_2@Fe-imidazole	Chlorpyrifos pesticide	Sensing (LOD = 2–10 ng mL^{-1})	167
12	$ZnFe_2O_4$/Fe–ZnO	VOC (acetone)	Sensing (response = 30.8–100 ppm)	90
13	CuO/Cu-MOF	Nitric oxide (NO)	Sensing (LOD = 7.8 nM)	168
14	Gr/MOF-GCE	Heavy metal ion sensing (As^{3+})	Sensing (LOD = 0.06 ppb)	169
19	Dy-MOF	Heavy metal ions (Pb^{2+} and Cu^{2+})	Langmuir adsorption (LOD = 0.4 μg L^{-1} [Pb^{2+}] and 0.264 μg L^{-1} [Cu^{2+}])	170
16	(MOF-NC)	Cu ions	Adsorption (q_e = 33.44 mg g^{-1})	171
17	(CDM6-K1000)	Antibiotics (ibuprofen, diclofenac)	Adsorption (ibuprofen = 408 mg g^{-1}) (diclofenac = 503 mg g^{-1}) isotherm = Langmuir	63
18	(Carbon–Fe/Fe$_3$C910)	Antibiotic (tetracycline)	Adsorption (511.06 mg g^{-1}) isotherm = Langmuir	172
19	ZIF-8@AG-CA	Organic contaminants	Adsorption (pore volume = 0.58 cm^3 g^{-1})	154
20	$Zn_{0.05}TiO_xN_y$@MOF-5	Heavy metal ion (Zn^{2+})	Adsorption and sensing (LOD = 0.0014 mg L^{-1}) isotherm = Langmuir and Freundlich	173

(carbon-Z), ZIF/sucrose (carbon-ZS), and ZIF/dicyandiamide (carbon-ZD) and synthesized three MOF-derived N-doped porous carbons.[147]

Due to their limitations, such as low activity after reuse and inevitable aggregation, MOFs produced relatively fewer examples of pure metal compounds as adsorbents than carbons. P-Al$_2$O$_3$ MSs (an innovative penetrable Al$_2$O$_3$ microsphere) were used to immobilize radionuclides (Eu(III) and U(VI)) from wastewater and performed much better than c-Al$_2$O$_3$ (commercial) nanomaterials in this process, showing energetic and excessive adsorption.[148] The uptake process can be explained by a variety of adsorption mechanisms, including hydrophobic, electrostatic, acid–base, p–p interaction, and H-bonding.[146,150] H-bond interaction is proposed as the primary cause of the extensive adsorption. Derivatives with distinctive structures require special attention. In addition, according to studies, the adsorptive efficiency of adsorbents was primarily dependent on the N and/or O species doping, i.e., heteroatom doping and the properties of the surface (e.g., porosity, pure volume, and BET area), which may be controlled by adding an external template or activating agent.[151,152] However, a more in-depth research is required to comprehend the adsorption mechanism because the effect of heteroatoms was not clearly demonstrated. A pore volume and larger surface area can make material transfer easier and make the active adsorption sites more visible, thus increasing the capture capacity.

The adsorption capacity is significantly influenced by the pore size and, in part, the species of the pollutants being absorbed. Micropores, for instance, are advantageous for MB adsorption and mesopores for TC capture.[153] However, the method for controlling the pore size remains a mystery. Specifically, the monopolized porous structure of the micropore has the inherent disadvantage of limited diffusion.[154] In short, using MOFs as precursors to create nanomaterials with remarkable functionalities could be an efficient way to boost their adsorption competitiveness in both industrial settings and academics, as shown in Table 1.

MOFs stand out in the field of drugs because of their remarkable adsorption properties. The MOF adsorption properties empower them to specifically adsorb and deliver drugs, prompting further developed drug viability and diminished secondary effects the productive expulsion of different drugs from the oceanic framework has been a considerable test due to the discrete physico-substance properties and less concentration.[155,156] Adsorption is one of the reassuring technologies for the effective removal of various pharmaceuticals from the water system because of its high elimination ability, fewer operation prices, and depletion in the emission of secondary dangerous pollutants.[157]

4. Conclusion & future perspective

In a nutshell, a critical appraisal of advancements in the field of nanotechnology associated with MOF as an environmental treatment has been undertaken herein. Owing to their tunable structure, enhanced surface area, and accessible electron-

transfer processes, MOF nanostructures are envisaged as a boon for ecosystem management. Restricting the size of MOFs in the nanoregime whether through the formation of nanocomposites or nanoparticles brings vast applicability to the versatility of MOFs. Herein, this review comprises various methods for the synthesis of MOF nanostructures along with their application as competent remedial agents for the removal of effluents from the environment.

The present review emphasized the synthetic modes of MOF nanocomposites or nanoparticles along with their applications as nanocatalysts, nanosensors, and nanoadsorbents. Several sensitive and selective applications involving the enhanced attributes of MOF nanostructures were classified and reviewed here.

Despite several advancements in the field of environmental detoxification using MOF nanostructures, there is some lag in their applicability. The prospects in this research area will be approached by following some localized purposes described here, which should be covered at the earliest.

(a) Surfactant molecules are generally employed for the stabilization and effective growth of MOF/MNPs composites, which can block the adsorption sites of MNPs by adsorbing on their surface. This adsorptive action could diminish the sensing attribute of such nanocomposites. Hence, more efficient strategies should be employed for the incorporation of MNPs on MOFs with controlled size and shape without using these surfactants.

(b) In MOF nanocomposites, using nanoscale MOF as a host is tedious and challenging. Generally, there is the employment of nanoparticles in the host MOFs rather than using MOF nanoparticles themselves for synthesizing nanocomposites. Removing this difficulty may put a milestone in the usability of MOF nanostructures.

(c) There should be certain advancements in long-term self-stability, e.g., photostability, thermal, and moisture stability of such MOF nanostructures, to improve their functionalization.

(d) To expand this field and enhance ecological balance, certain technologies should be linked with these nanostructures. Combination with paper chips and test strips can make MOF nanostructures suitable sensors for heavy metal ions and can be used in portable devices.

(e) Correlating MOF nanostructures with optical, plasmonic, and electronic fields can improve their catalytic and sensing performance using electrochemical principles.

(f) In most research works, self-prepared laboratory samples are used; therefore, real environmental samples should be tested to exactly determine the usefulness of the developed methods at the ground level.

(g) The quantum yield obtained for the nanostructures should be improved by synthetic modifications. Yield should be enough to use these in industrial applications for the large-scale decontamination of aqueous and air contaminants.

Last but not least, despite having some challenges pending resolution, MOF nanostructures have a brilliant future ahead. This area with minor advancements can further open up an avenue for the maintenance of a healthy environment and ecological stability. The restorative approach that it carries for the decontamination of environmental toxicity is the root cause for the extension of this work for the betterment of our flourishing environment.

Author contributions

Indu Sharma – writing, drafting and data collection; Jaspreet Kaur – drafting and analysing; Gargi Poonia – data collection and writing; Surinder Kumar Mehta – analysing and proofreading; Ramesh Kataria – conceptualisation, analysing and proof-reading.

Conflicts of interest

There are no conflicts to declare.

Acknowledgements

References

1 J. Darabdhara and M. Ahmaruzzaman, *Chemosphere*, 2022, **304**, 135261.

2 S. Mosleh, M. R. Rahimi, M. Ghaedi, K. Dashtian and S. Hajati, *RSC Adv*, 2016, **6**, 63667–63680.

3 A. J. Ebele, M. Abou-Elwafa Abdallah and S. Harrad, *Emerg. Contam.*, 2017, **3**, 1–16.

4 M. Oves, M. Z. Khan and I. M. I. Ismail, *Mod. Age Environ. Probl. their Remediat.*, 2017, 1–237.

5 I. B. Gomes, L. C. Simões and M. Simões, *Sci. Total Environ.*, 2018, **643**, 1348–1356.

6 N. S. Thomaidis, A. G. Asimakopoulos and A. A. Bletsou, *Glob. Nest J.*, 2012, **14**, 72–79.

7 T. Rasheed, M. Bilal, F. Nabeel, M. Adeel and H. M. N. Iqbal, *Environ. Int.*, 2019, **122**, 52–66.

8 J. L. Wilkinson, P. S. Hooda, J. Barker, S. Barton and J. Swinden, *Crit. Rev. Environ. Sci. Technol.*, 2016, **46**, 336–381.

9 M. Safaei, M. M. Foroughi, N. Ebrahimpoor, S. Jahani, A. Omidi and M. Khatami, *TrAC - Trends Anal. Chem.*, 2019, **118**, 401–425.

10 S. Kader, M. O. Raimi, V. Spalevic, I. Asomeji and W. B. Raheem, *Manuscr. Draft*, 2023, **2301011**, 1–10.

11 P. Kumar, A. Deep and K. H. Kim, *TrAC - Trends Anal. Chem.*, 2015, **73**, 39–53.

12 L. Qiu, C. Yu, X. Wang, Y. Xie, A. M. Kirillov, W. Huang, J. Li, P. Gao, T. Wu, X. Gu, Q. Nie and D. Wu, *Inorg. Chem.*, 2019, **58**, 4524–4533.

13 Y. Wang, C. Pan, W. Chu, A. K. Vipin and L. Sun, *Nanomaterials*, 2019, **9**, 439.

14 S. Subudhi, S. P. Tripathy and K. Parida, *Inorg. Chem. Front.*, 2021, **8**, 1619–1636.

15 A. Malik, M. Nath, S. Mohiyuddin and G. Packirisamy, *ACS Omega*, 2018, **3**, 8288–8308.

16 R. Dolas, C. Saravanan and B. P. Kaur, *Ultrason. Sonochem.*, 2019, **58**, 104609.

17 O. Azizabadi, F. Akbarzadeh, S. Danshina, N. P. S. Chauhan and G. Sargazi, *J. Solid State Chem.*, 2021, **294**, 121897.

18 F. Israr, D. K. Kim, Y. Kim, S. J. Oh, K. C. Ng and W. Chun, *Ultrason. Sonochem.*, 2016, **29**, 186–193.

19 S. Li, L. Tan and X. Meng, *Adv. Funct. Mater.*, 2020, **30**, 1–26.

20 T. Chalati, P. Horcajada, R. Gref, P. Couvreur and C. Serre, *J. Mater. Chem.*, 2011, **21**, 2220–2227.

21 G. Sargazi, D. Afzali and A. Mostafavi, *J. Porous Mater.*, 2018, **25**, 1723–1741.

22 M. V. Varsha and G. Nageswaran, *J. Electrochem. Soc.*, 2020, **167**, 155527.

23 O. J. De Lima Neto, A. C. d. O. Frós, B. S. Barros, A. F. De Farias Monteiro and J. Kulesza, *New J. Chem.*, 2019, **43**, 5518–5524.

24 F. Zhang, T. Zhang, X. Zou, X. Liang, G. Zhu and F. Qu, *Solid State Ionics*, 2017, **301**, 125–132.

25 H. M. Yang, X. Liu, X. L. Song, T. L. Yang, Z. H. Liang and C. M. Fan, *Trans. Nonferrous Met. Soc. China*, 2015, **25**, 3987–3994.

26 J. Z. Wei, F. X. Gong, X. J. Sun, Y. Li, T. Zhang, X. J. Zhao and F. M. Zhang, *Inorg. Chem.*, 2019, **58**, 6742–6747.

27 A. Pandey, N. Dhas, P. Deshmukh, C. Caro, P. Patil, M. Luisa García-Martín, B. Padya, A. Nikam, T. Mehta and S. Mutalik, *Coord. Chem. Rev.*, 2020, **409**, 213212.

28 J. Z. Wei, X. L. Wang, X. J. Sun, Y. Hou, X. Zhang, D. D. Yang, H. Dong and F. M. Zhang, *Inorg. Chem.*, 2018, **57**, 3818–3824.

29 E. M. C. Morales, M. A. Méndez-Rojas, L. M. Torres-Martínez, L. F. Garay-Rodríguez, I. López, I. E. Uflyand and B. I. Kharisov, *Polyhedron*, 2021, **210**, 1–7.

30 A. Schaate, P. Roy, A. Godt, J. Lippke, F. Waltz, M. Wiebcke and P. Behrens, *Chem.–Eur. J.*, 2011, **17**, 6643–6651.

31 S. A. A. Razavi, M. Y. Masoomi and A. Morsali, *Ultrason. Sonochem.*, 2017, **37**, 502–508.

32 L. G. Qiu, Z. Q. Li, Y. Wu, W. Wang, T. Xu and X. Jiang, *Chem. Commun.*, 2008, **31**, 3642–3644.

33 M. Y. Masoomi, A. Morsali and P. C. Junk, *RSC Adv*, 2014, **4**, 47894–47898.

34 Z. Luo, S. Fan, C. Gu, W. Liu, J. Chen, B. Li and J. Liu, *Curr Med Chem*, 2019, 3341–3369.

35 N. Stock and S. Biswas, *Chem. Rev.*, 2012, **112**, 933–969.

36 K. M. Ø. Jensen, C. Tyrsted, M. Bremholm and B. B. Iversen, *ChemSusChem*, 2014, **7**, 1–19.

37 Y. Huo, S. Xiu, L. Meng and B. Quan, *Chem. Eng. J.*, 2023, **451**, 138572.

38 R. L. Barns, E. D. Kolb, R. A. Laudise, E. E. Simpson and K. M. Kroupa, *J. Cryst. Growth*, 1976, **34**, 189–197.

39 M. Miyamoto, S. Kohmura, H. Iwatsuka, Y. Oumi and S. Uemiya, *CrystEngComm*, 2015, **17**, 3422–3425.

40 B. A. Rabenau, *Angew. Chem.*, 1985, **24**, 1026–1040.

41 J. Mira, *J. Solid State Chem.*, 2009, **182**, 2685–2690.

42 T. He, D. Chen, X. Jiao, Y. Xu and Y. Gu, *Langmuir*, 2004, **20**, 8404–8408.

43 S. Assemblies, *Angew Chem*, 2003, **43**, 2872–2875.

44 Y. Xu, M. Xie, X. Li, F. Shao, S. Li, S. Li, Y. Xu, J. Chen, F. Zeng and Y. Jiao, *J. Colloid Interface Sci.*, 2022, **626**, 426–434.

45 S. Aslam, J. Zeng, F. Subhan, M. Li, F. Lyu, Y. Li and Z. Yan, *J. Colloid Interface Sci.*, 2017, **505**, 186–195.

46 S. Zheng, Q. Li, H. Xue, H. Pang and Q. Xu, *Natl. Sci. Rev.*, 2020, **7**, 305–314.

47 V. J. Ariyamparambil and B. Kandasubramanian, *Chem. Eng. J. Adv.*, 2022, **11**, 100355.

48 M. A. Al-Baadani, L. Xu, K. Hii Ru Yie, A. Sun, X. Gao, K. Cai, B. A. Al-Shaaobi, A. M. Al-Bishari, L. Cai, X. Shen, J. Liu and P. Ma, *Mater. Des.*, 2022, **217**, 110596.

49 H. R. Moon, D. W. Lim and M. P. Suh, *Chem. Soc. Rev.*, 2013, **42**, 1807–1824.

50 A. Aijaz and Q. Xu, *J. Phys. Chem. Lett.*, 2014, **5**, 1400–1411.

51 H. Wang, J. Zhao, C. Liu, Y. Tong and W. He, *ACS Omega*, 2021, **6**, 4807–4815.

52 S. Guo, L. Chi, T. Zhao, Y. Nan, X. Sun, Y. Huang, B. Hou and X. Wang, *J. Electroanal. Chem.*, 2021, **880**, 114915.

53 J. H. Zhao, Y. Wang, X. Tang, Y. H. Li, F. T. Liu, Y. Zhang and K. Li, *Dalt. Trans.*, 2019, **48**, 3560–3565.

54 K. Kumagai, T. Uematsu, T. Torimoto and S. Kuwabata, *Chem. Mater.*, 2021, **33**, 1607–1617.

55 T. Noor, N. Zaman, H. Nasir, N. Iqbal and Z. Hussain, *Electrochim. Acta*, 2019, **307**, 1–12.

56 E. Akbarzadeh, H. Z. Soheili, M. Hosseinifard and M. R. Gholami, *Mater. Res. Bull.*, 2020, **121**, 110621.

57 W. Xia, J. Zhu, W. Guo, L. An, D. Xia and R. Zou, *J. Mater. Chem. A*, 2014, **2**, 11606–11613.

58 Z. Xiang, Y. Song, J. Xiong, Z. Pan, X. Wang, L. Liu, R. Liu, H. Yang and W. Lu, *Carbon*, 2019, **142**, 20–31.

59 S. Wang, Y. Hou, S. Lin and X. Wang, *Nanoscale*, 2014, **6**, 9930–9934.

60 J. Qin, J. Wang, J. Yang, Y. Hu, M. Fu and D. Ye, *Appl. Catal. B Environ.*, 2020, **267**, 118667.

61 S. Ye, M. Yan, X. Tan, J. Liang, G. Zeng, H. Wu, B. Song, C. Zhou, Y. Yang and H. Wang, *Appl. Catal. B Environ.*, 2019, **250**, 78–88.

62 H. Yi, M. Yan, D. Huang, G. Zeng, C. Lai, M. Li, X. Huo, L. Qin, S. Liu, X. Liu, B. Li, H. Wang, M. Shen, Y. Fu and X. Guo, *Appl. Catal. B Environ.*, 2019, **250**, 52–62.

63 I. I. Alkhatib, C. Garlisi, M. Pagliaro, K. Al-Ali and G. Palmisano, *Catal. Today*, 2020, **340**, 209–224.

64 H. Robatjazi, D. Weinberg, D. F. Swearer, C. Jacobson, M. Zhang, S. Tian, L. Zhou, P. Nordlander and N. J. Halas, *Sci. Adv.*, 2019, **5**, 1–11.

65 J. Becerra, D. T. Nguyen, V. N. Gopalakrishnan and T. O. Do, *ACS Appl. Energy Mater.*, 2020, **3**, 7659–7665.

66 F. Guo, Y. P. Wei, S. Q. Wang, X. Y. Zhang, F. M. Wang and W. Y. Sun, *J. Mater. Chem. A*, 2019, **7**, 26490–26495.

67 Y. Huang, Y. Zhang, X. Chen, D. Wu, Z. Yi and R. Cao, *Chem. Commun.*, 2014, **50**, 10115–10117.

68 C. Venkata, K. Raghava, V. V. N. Harish, J. Shim, M. V Shankar, N. P. Shetti and T. M. Aminabhavi, *Int. J. Hydrogen Energy*, 2019, **45**, 7656–7679.

69 R. Liang, F. Jing, L. Shen, N. Qin and L. Wu, *Nano Res*, 2015, **8**, 3237–3249.

70 B. Hu, J. Y. Yuan, J. Y. Tian, M. Wang, X. Wang, L. He, Z. Zhang, Z. W. Wang and C. Sen Liu, *J. Colloid Interface Sci.*, 2018, **531**, 148–159.

71 Y. Lei, C. S. Chen, Y. J. Tu, Y. H. Huang and H. Zhang, *Environ. Sci. Technol.*, 2015, **49**, 6838–6845.

72 Z. Ye, J. A. Padilla, E. Xuriguera, E. Brillas and I. Sirés, *Appl. Catal. B Environ.*, 2020, **266**, 118604.

73 Y. Yao, H. Chen, C. Lian, F. Wei, D. Zhang, G. Wu, B. Chen and S. Wang, *J. Hazard. Mater.*, 2016, **314**, 129–139.

74 J. Tang and J. Wang, *Chem. Eng. J.*, 2019, **375**, 122007.

75 C. Wang, H. Wang, R. Luo, C. Liu, J. Li, X. Sun, J. Shen, W. Han and L. Wang, *Chem. Eng. J.*, 2017, **330**, 262–271.

76 Y. Du and X. Han, *J. Mater. Chem. A*, 2018, 3.

77 G. Yilmaz, C. F. Tan, M. Hong and G. W. Ho, *Adv. Funct. Mater.*, 2017, **1704177**, 1–9.

78 W. Oh, Z. Dong and T. Lim, *Applied Catal. B Environ.*, 2016, **194**, 169–201.

79 L. Chen, X. Zuo, S. Yang, T. Cai and D. Ding, *Chem. Eng. J.*, 2019, **359**, 373–384.

80 P. Ji, J. B. Solomon, Z. Lin, A. M. Wilders, R. F. Jordan and W. Lin, *J. Am. Chem. Soc.*, 2017, **139**, 11325–11328.

81 H. Li, B. Xu, J. He, X. Liu, W. Gao and Y. Mu, *Chem. Commun.*, 2015, **51**, 16703–16706.

82 S. Pal, S. S. Yu and C. W. Kung, *Chemosensors*, 2021, **9**, 306.

83 L. E. Kreno, K. Leong, O. K. Farha, M. Allendorf, R. P. Van Duyne and J. T. Hupp, *Chem. Rev.*, 2012, **112**, 1105–1125.

84 X. Fang, B. Zong and S. Mao, *Nano-Micro Lett.*, 2018, **10**, 1–19.

85 G. Gumilar, Y. V. Kaneti, J. Henzie, S. Chatterjee, J. Na, B. Yuliarto, N. Nugraha, A. Patah, A. Bhaumik and Y. Yamauchi, *Chem. Sci.*, 2020, **11**, 3644–3655.

86 J. Xu, J. Ma, Y. Peng, S. Cao, S. Zhang and H. Pang, *Chinese Chem. Lett.*, 2023, **34**, 107527.

87 S. Homayoonnia and S. Zeinali, *Sensors Actuators, B Chem.*, 2016, **237**, 776–786.

88 P. Mochalski, J. King, M. Klieber, K. Unterkofler, H. Hinterhuber, M. Baumann and A. Amann, *Analyst*, 2013, **138**, 2134–2145.

89 H. H. Yeung, G. Yoshikawa, K. Minami and K. Shiba, *J. Mater. Chem. A*, 2020, **8**, 18007–18014.

90 E. Cao, Z. Guo, G. Song, Y. Zhang, W. Hao and L. Sun, *Sensors Actuators B. Chem.*, 2020, **325**, 128783.

91 C. Zhang, L. Sun, Y. Yan, Y. Liu, Z. Liang, Y. Liu and J. Li, *J. Mater. Chem. C*, 2017, **5**, 2084–2089.

92 W. Shi, F. Xing, Y. L. Bai, M. Hu, Y. Zhao, M. X. Li and S. Zhu, *ACS Appl. Mater. Interfaces*, 2015, **7**, 14493–14500.

93 L. F. Wang, W. M. Zhuang, G. Z. Huang, Y. C. Chen, J. Z. Qiu, Z. P. Ni and M. L. Tong, *Chem. Sci.*, 2019, **10**, 7496–7502.

94 H. Y. Li, S. N. Zhao, S. Q. Zang and J. Li, *Chem. Soc. Rev.*, 2020, **49**, 6364–6401.

95 H. Sohrabi, P. Salahshour Sani, Y. Orooji, M. R. Majidi, Y. Yoon and A. Khataee, *Food Chem. Toxicol.*, 2022, **165**, 113176.

96 Q. Yang, J. Wang, X. Chen, W. Yang, H. Pei, N. Hu, Z. Li, Y. Suo, T. Li and J. Wang, *J. Mater. Chem. A*, 2018, **6**, 2184–2192.

97 L. Ma, Y. He, Y. Wang, Y. Wang, R. Li, Z. Huang, Y. Jiang and J. Gao, *Electrochim. Acta*, 2019, **318**, 525–533.

98 X. Li, X. Gao, P. Gai, X. Liu and F. Li, *Sensors Actuators, B Chem.*, 2020, **323**, 128701.

99 S. Niazipour, J. B. Raoof and M. Ghani, *J. Chromatogr. A*, 2021, **1660**, 462677.

100 M. Wagner, K. Y. Andrew Lin, W. Da Oh and G. Lisak, *J. Hazard. Mater.*, 2021, **413**, 1–8.

101 M. Wagner, K. Y. Andrew Lin, W. Da Oh and G. Lisak, *J. Hazard. Mater.*, 2021, **413**, 125345.

102 W.-T. Koo, J.-S. Jang and I.-D. Kim, *Chem*, 2019, **5**, 1938–1963.

103 P. Kumar, K. H. Kim, V. Bansal, T. Lazarides and N. Kumar, *J. Ind. Eng. Chem.*, 2017, **54**, 30–43.

104 B. Liu, W. P. Wu, L. Hou and Y. Y. Wang, *Chem. Commun.*, 2014, **50**, 8731–8734.

105 F. F. Wang, C. Liu, J. Yang, H. L. Xu, W. Y. Pei and J. F. Ma, *Chem. Eng. J.*, 2022, **438**, 135639.

106 Y. Wang, L. Wang, W. Huang, T. Zhang, X. Hu, J. A. Perman and S. Ma, *J. Mater. Chem. A*, 2017, **5**, 8385–8393.

107 W. Shi, M. He, W. Li, X. Wei, B. Bui, M. Chen and W. Chen, *ACS Appl. Nano Mater.*, 2021, **4**, 802–810.

108 X. Wang, H. Wang, L. Guo, G. Chen, R. Kong, F. Qu and L. Xia, *Analyst*, 2020, **145**, 1362–1367.

109 S. Bhattacharjee, S. Bera, R. Das, D. Chakraborty, A. Basu, P. Banerjee, S. Ghosh and A. Bhaumik, *ACS Appl. Mater. Interfaces*, 2022, **14**, 20907–20918.

110 S. Tian, C. Zhang, D. Huang, R. Wang, G. Zeng, M. Yan, W. Xiong, C. Zhou, M. Cheng, W. Xue and Y. Yang, *Chem. Eng. J.*, 2020, **389**, 123423.

111 H. Li, Y. Li, B. Li, D. Liu and Y. Zhou, *Chemosphere*, 2012, **89**, 1307–1315.

112 M. Barczak, R. Dobrowolski, P. Borowski and D. A. Giannakoudakis, *Microporous Mesoporous Mater*, 2020, **299**, 110132.

113 S. Huang, W. Deng, L. Zhang, D. Yang and Q. Gao, *Microporous Mesoporous Mater*, 2020, **302**, 110204.

114 A. Modak, P. Bhanja, M. Selvaraj and A. Bhaumik, *Environ. Sci. Nano*, 2020, **7**, 2887–2923.

115 S. Das, S. Chatterjee, S. Mondal, A. Modak, B. K. Chandra, S. Das, G. D. Nessim, A. Majee and A. Bhaumik, *Chem. Commun.*, 2020, **56**, 3963–3966.

116 J. He, Y. Xu, W. Wang, B. Hu, Z. Wang, X. Yang, Y. Wang and L. Yang, *Arab. J. Chem.*, 2022, **15**, 103955.

117 Z. Luo, Y. He, D. Zhi, L. Luo, Y. Sun, E. Khan, L. Wang, Y. Peng, Y. Zhou and D. C. W. Tsang, *Sci. Total Environ.*, 2019, **696**, 133990.

118 Y. Zhou, Y. He, Y. Xiang, S. Meng, X. Liu, J. Yu, J. Yang, J. Zhang, P. Qin and L. Luo, *Sci. Total Environ.*, 2019, **646**, 29–36.

119 L. Huang, R. Shen and Q. Shuai, *J. Environ. Manage.*, 2021, **277**, 111389.

120 L. Li, X. L. Liu, H. Y. Geng, B. Hu, G. W. Song and Z. S. Xu, *J. Mater. Chem. A*, 2013, **1**, 10292–10299.

121 W. Zhang, Y. Hu, J. Ge, H. L. Jiang and S. H. Yu, *J. Am. Chem. Soc.*, 2014, **136**, 16978–16981.

122 Z. Hasan and S. H. Jhung, *J. Hazard. Mater.*, 2015, **283**, 329–339.

123 B. Van De Voorde, B. Bueken, J. Denayer and D. De Vos, *Chem. Soc. Rev.*, 2014, **43**, 5766–5788.

124 H. Furukawa, K. E. Cordova, M. O'Keeffe and O. M. Yaghi, *Science*, 2013, **341**, 1230444.

125 Z. Zhao, X. Li, S. Huang, Q. Xia and Z. Li, *Ind. Eng. Chem. Res.*, 2011, **50**, 2254–2261.

126 M. P. Suh, H. J. Park, T. K. Prasad and D. W. Lim, *Chem. Rev.*, 2012, **112**, 782–835.

127 K. Lu, T. Aung, N. Guo, R. Weichselbaum and W. Lin, *Adv. Mater.*, 2018, **30**, 1–20.

128 Y. N. Wu, M. Zhou, B. Zhang, B. Wu, J. Li, J. Qiao, X. Guan and F. Li, *Nanoscale*, 2014, **6**, 1105–1112.

129 H. Saleem, U. Rafique and R. P. Davies, *Microporous Mesoporous Mater*, 2016, **221**, 238–244.

130 B. Li, H. M. Wen, Y. Cui, W. Zhou, G. Qian and B. Chen, *Adv. Mater.*, 2016, **28**, 8819–8860.

131 B. Szczęśniak, J. Choma and M. Jaroniec, *J. Colloid Interface Sci.*, 2018, **514**, 801–813.

132 S. Cai, W. Li, P. Xu, X. Xia, H. Yu, S. Zhang and X. Li, *Analyst*, 2019, **144**, 3729–3735.

133 M. Manoochehri and M. Mehraban, *RSC*, 2018, **42**, 17636–17643.

134 M. R. Sohrabi and Z. Matbouie, *Microchemica Acta*, 2013, **180**, 589–597.

135 Y. Wu, G. Xu, W. Liu, J. Yang, F. Wei, L. Li and W. Zhang, *Microporous Mesoporous Mater*, 2015, **210**, 110–115.

136 F. Ke, J. Jiang, Y. Li, J. Liang, X. Wan and S. Ko, *Appl. Surf. Sci.*, 2017, **413**, 266–274.

137 T. Rasheed, M. Bilal, A. Ahmad, F. Nabeel, R. Naresh, L. Fernando, R. Ferreira, H. Nguyen and H. M. N. Iqbal, *Environ. Res.*, 2020, **185**, 109436.

138 P. Zhao, N. Liu, C. Jin, H. Chen, Z. Zhang, L. Zhao, P. Cheng and Y. Chen, *Inorg. Chem.*, 2019, **58**, 8787–8792.

139 S. Lin, Y. Zhao and Y. S. Yun, *ACS Appl. Mater. Interfaces*, 2018, **10**, 28076–28085.

140 I. Ahmed, B. N. Bhadra, H. J. Lee and S. H. Jhung, *Catal. Today*, 2018, **301**, 90–97.

141 S. Lin, Y. Zhao and Y. Yun, *ACS Appld Mater Interfaces*, 2018, **10**, 28076–28085.

142 A. C. Tella, S. O. Owalude, S. J. Olatunji, V. O. Adimula, S. E. Elaigwu, L. O. Alimi, P. A. Ajibade and O. S. Oluwafemi, *J. Environ. Sci.*, 2017, **64**, 264–275.

143 T. Xuan, V. Hung, S. Thanh and H. Choi, *J. Hazard. Mater.*, 2013, **254–255**, 345–353.

144 P. Taylor, S. Saha, U. Sarkar and S. Mondal, *Phys Rev Lett*, 2018, **125**, 151802.

145 B. N. Bhadra and S. H. Jhung, *Microporous Mesoporous Mater*, 2018, **270**, 102–108.

146 B. N. Bhadra, J. K. Lee, C. Cho and S. H. Jhung, *J. Chem. Eng.*, 2018, **343**, 225–234.

147 S. Xu, Y. Lv, X. Zeng and D. Cao, *Chem. Eng. J.*, 2017, **323**, 502–511.

148 S. Huang, H. Pang, L. Li, S. Jiang, T. Wen, L. Zhuang and B. Hu, *Chem. Eng. J.*, 2018, **353**, 157–166.

149 I. Ahmed, T. Panja, N. A. Khan, M. Sarker, J. Yu, S. H. Jhung and J. Yu, *ACS Appl. Mater. Interfaces*, 2017, **9**, 10276–10285.

150 H. J. An, B. N. Bhadra, N. A. Khan and S. H. Jhung, *Chem. Eng. J.*, 2018, **343**, 447–454.

151 B. N. Bhadra and S. H. Jhung, *J. Hazard. Mater.*, 2017, **340**, 179–188.

152 B. N. Bhadra, I. Ahmed, S. Kim and S. H. Jhung, *Chem. Eng. J.*, 2017, **314**, 50–58.

153 E. Article, Q. Wen, J. Di, Y. Zhao, Y. Wang and J. Yu, *Chem. Sci.*, 2013, **4**, 4378–4382.

154 C. Wang, J. Kim, J. Tang, J. Na, Y. M. Kang, M. Kim, H. Lim, Y. Bando, J. Li and Y. Yamauchi, *Angew. Chemie - Int. Ed.*, 2020, **59**, 2066–2070.

155 K. G. Pavithra, P. Senthil Kumar, P. Sundar Rajan, A. Saravanan and M. Naushad, *Korean J. Chem. Eng.*, 2017, **34**, 2787–2805.

156 M. B. Cristóvão, R. Janssens, A. Yadav, S. Pandey, P. Luis, B. Van der Bruggen, K. K. Dubey, M. K. Mandal, J. G. Crespo and V. J. Pereira, *J. Hazard. Mater.*, 2020, **392**, 122330.

157 Y. Xu, T. Liu, Y. Zhang, F. Ge, R. M. Steel and L. Sun, *J. Mater. Chem. A*, 2017, **5**, 12001–12014.

158 D. Chen, S. Chen, Y. Jiang, S. Xie, H. Quan, X. Luo and L. Guo, *RSC Adv*, 2017, **7**, 49024–49030.

159 S. Zhang, H. Gao, X. Xu, R. Cao, H. Yang, X. Xu and J. Li, *Chem. Eng. J.*, 2020, **381**, 122670.

160 B. Hashemzadeh, H. Alamgholiloo, N. Noroozi Pesyan, E. Asgari, A. Sheikhmohammadi, J. Yeganeh and H. Hashemzadeh, *Chemosphere*, 2021, **281**, 130970.

161 X. Chen, X. Chen, S. Cai, J. Chen, W. Xu, H. Jia and J. Chen, *Chem. Eng. J.*, 2018, **334**, 768–779.

162 Y. Wen, R. Li, J. Liu, X. Zhang, P. Wang, X. Zhang, B. Zhou, H. Li, J. Wang, Z. Li and B. Sun, *Anal. Chim. Acta*, 2020, **1127**, 131–139.

163 W. Zhou, Y. P. Wu, J. Zhao, W. W. Dong, X. Q. Qiao, D. F. Hou, X. Bu and D. S. Li, *Inorg. Chem.*, 2017, **56**, 14111–14117.

164 R. Kaur, A. K. Paul and A. Deep, *Forensic Sci. Int.*, 2014, **242**, 88–93.

165 H. Karimi-Maleh, M. L. Yola, N. Atar, Y. Orooji, F. Karimi, P. Senthil Kumar, J. Rouhi and M. Baghayeri, *J. Colloid Interface Sci.*, 2021, **592**, 174–185.

166 W. Ye, Y. Li, J. Wang, B. Li, Y. Cui, Y. Yang and G. Qian, *J. Solid State Chem.*, 2020, **281**, 121032.

167 P. Arulpriya, T. Krishnaveni, T. Shanmugasundaram and K. Kadirvelu, *J. Ind. Eng. Chem.*, 2022, **112**, 146–161.

168 N. Alizadeh, A. Salimi and T. K. Sham, *Microchim. Acta*, 2021, **188**, 1–11.

169 M. Baghayeri, M. Ghanei-Motlagh, R. Tayebee, M. Fayazi and F. Narenji, *Anal. Chim. Acta*, 2020, **1099**, 60–67.

170 A. Jamali, A. A. Tehrani, F. Shemirani and A. Morsali, *Dalt. Trans.*, 2016, **45**, 9193–9200.

171 N. Bakhtiari, S. Azizian, S. M. Alshehri, N. L. Torad, V. Malgras and Y. Yamauchi, *Microporous Mesoporous Mater*, 2015, **217**, 173–177.

172 W. Xiong, Z. Zeng, G. Zeng, Z. Yang, R. Xiao, X. Li, J. Cao, C. Zhou, H. Chen, M. Jia, Y. Yang, W. Wang and X. Tang, *Chem. Eng. J.*, 2019, **374**, 91–99.

173 S. A. Younis, T. A. Ali and P. Serp, *J. Environ. Chem. Eng.*, 2021, **9**, 106186.